Selective STING stimulation in dendritic cells primes antitumor T cell responses

Bakhos Jneid, Aurore Bochnakian, Caroline Hoffmann, Fabien Delisle, Emeline Djacoto, Philémon Sirven, Jordan Denizeau, Christine Sedlik, Yohan Gerber-Ferder, Frédéric Fiore, et al.

Accepted version of the following manuscript published in Science Immunology

Jneid B, Bochnakian A, Hoffmann C, Delisle F, Djacoto E, Sirven P, Denizeau J, Sedlik C, Gerber-Ferder Y, Fiore F, Akyol R, Brousse C, Kramer R, Walters I, Carlioz S, Salmon H, Malissen B, Dalod M, Piaggio E, Manel N. Selective STING stimulation in dendritic cells primes antitumor T cell responses. Sci Immunol. 2023 Jan 13;8(79):eabn6612. doi: 10.1126/sciimmunol.abn6612. PMID: 36638189.

The published version of the manuscript can be accessed on the Journal website:
https://www.science.org/doi/10.1126/sciimmunol.abn6612

Selective STING stimulation in dendritic cells primes anti-tumor T cell responses

Bakhos Jneid[1], Aurore Bochnakian[1,2], Caroline Hoffmann[3], Fabien Delisle[1], Emeline Djacoto[1], Philémon Sirven[1], Jordan Denizeau[1], Christine Sedlik[1], Yohan Gerber-Ferder[1], Frédéric Fiore[4], Ramazan Akyol[5], Carine Brousse[5], Robert Kramer[2], Ian Walters[2], Sylvain Carlioz[2], Hélène Salmon[1], Bernard Malissen[4], Marc Dalod[5], Eliane Piaggio[1], Nicolas Manel[1,*]

[1] Institut Curie, PSL Research University, INSERM U932, Paris, France.

[2] Stimunity, Paris, France.

[3] Institut Curie, INSERM U932 Immunity and Cancer, Department of Surgical Oncology, PSL University, Paris, France.

[4] Centre d'Immunophénomique (CIPHE), Aix Marseille Université, INSERM, CNRS, 13288 Marseille, France

[5] Aix-Marseille University, CNRS, INSERM, CIML, Centre d'Immunologie de Marseille-Luminy, Turing Center for Living Systems, Marseille, France.

* Correspondance: nicolas.manel@curie.fr

Abstract

T cells that recognize tumor antigens are crucial for anti-tumor immune responses. Induction of anti-tumor T cells in immunogenic tumors depends on STING, the intracellular innate immune receptor for cyclic guanosine monophosphate-adenosine monophosphate (cGAMP) and related cyclic dinucleotides (CDNs). However, the optimal way to leverage STING activation in non-immunogenic tumors is still unclear. Here, we show that cGAMP delivery by intra-tumoral injection of virus-like particles (cGAMP-VLP) led to differentiation of circulating tumor-specific T cells, decrease in tumor regulatory T cells (Tregs) and anti-tumoral responses that synergize with PD1 blockade. By contrast, intra-tumoral injection of the synthetic CDN ADU-S100 led to tumor necrosis and systemic T cell activation but simultaneously depleted immune cells from injected tumors and induced minimal priming of circulating tumor-specific T cells. The anti-tumor effects of cGAMP-VLP required type 1 conventional dendritic cells (cDC1), while ADU-S100 eliminated cDC1 from injected tumors. cGAMP-VLP preferentially targeted STING in dendritic cells at a 1000-fold less dose than ADU-S100. Sub-cutaneous administration of cGAMP-VLP showed synergy when combined with PD1 blockade or a tumor Treg-depleting antibody to elicit systemic tumor-specific T cells and anti-tumor activity, leading to complete and durable tumor eradication in the case of tumor Treg depletion. These findings show that cell targeting of STING stimulation shapes the anti-tumor T cell response and reveal a therapeutic strategy with T cell modulators.

One-sentence summary (150 char):

STING stimulation by virus-like particles activates anti-tumor immunity more effectively than a non-targeted synthetic STING agonist.

Introduction

T cells that recognize tumor antigens are critical effectors of the anti-tumor immune response. Most cancer patients do not naturally mount effective T cell responses against their tumors, but the emergence of immune-checkpoint blocking antibodies (ICB) has led to remarkable therapeutic success, albeit in a fraction of patients and tumor types. ICB require pre-existing anti-tumor T cells responses to effectively stimulate subsequent anti-tumor immune responses *(1)*. The understanding of the mechanisms that efficiently generate anti-tumor T cells has the potential to expand the efficacy of ICB by enabling new classes of immunotherapeutic agents.

Specialized antigen presenting-cells can stimulate T cell responses from naive cells. Antigen-presenting cells are activated by innate immune signals emanating from germline-encoded pattern recognition receptors that recognize non-self or altered-self molecules. STING is an intracellular pattern recognition receptor for cyclic dinucleotides (CDNs) implicated in the response to bacteria and to intracellular DNA of foreign and altered-self origins. In mouse models, spontaneous generation of anti-tumor T cells against immunogenic tumors has been shown to rely on STING activation *(2)*. Intra-tumoral injection of synthetic CDNs that activate STING stimulate anti-tumor responses, but the underlying mechanisms remain unclear *(3)*. In fact, synthetic CDNs can have contradictory immune-stimulatory and immuno-ablative effects at different doses *(4)*. Given that STING is broadly expressed in normal tissues and also tumors, the potential for tissue-specific activation of STING may either support protective or pathological responses *(5)*. For example, STING activation within T cells inhibits their proliferation and, at least in mouse, triggers their death by apoptosis *(6, 7)*. The specific cell types in which STING activation must occur to optimally prime antigen-specific anti-tumor T cell responses is unknown.

In addition to roles in tumor immunity, the STING pathway also plays an evolutionary conserved role in anti-viral immunity *(8, 9)*. Moreover, the natural mammalian STING agonist,

2'3'-cGAMP (cGAMP) can be packaged in particles of enveloped viruses, leading to STING activation in target cells immediately after fusion of the viral particles *(10, 11)*. This represents a Trojan horse system of antiviral defense without the need to detect viral nucleic acids. Consequently, cGAMP can be packaged in non-infectious enveloped virus-like particles (VLP). These enveloped retroviral VLPs can be readily produced and purified, enabling the production of cGAMP-containing VLPs (cGAMP-VLP) *(10, 11)*. Inclusion of cGAMP enhances the immunogenicity of VLPs displaying influenza virus or SARS-CoV-2 glycoproteins *(12)*.

Here, we leveraged the biological properties of cGAMP-VLP to investigate anti-tumoral immunity induced by STING activation. We characterized STING activation *in vivo* by cGAMP-VLP compared to established synthetic cyclic dinucleotide (CDN). Using cGAMP-VLP, we show that STING is essential in dendritic cells for the induction of tumor-specific T cell responses that respond to ICB. Finally, we identify a critical role of tumor Treg in limiting anti-tumor T cell response induced by STING activation.

Results

Production and characterization of cGAMP-VLP

cGAMP-VLP is composed of HIV-1 structural proteins and VSV-G envelope glycoprotein. cGAMP is incorporated in VLPs as a result of cGAS expression in producer cells and activation by the transfected plasmid DNA. We generated cGAMP-VLP by transient transfection of 293FT cells and subsequently purified them through a sucrose cushion and two rounds of ultra-centrifugation. We routinely measured the concentration of cGAMP and of p24 (antigen of the structural viral protein Gag of HIV-1 used to produce the VLP) in the purified preparations. Using a nanoparticle tracker, we observed a homogenous distribution average size of 158 nm, which is consistent with the size of retroviral particles (**Figure S1A**). We visualized the cGAMP-VLP by electron microscopy, which confirmed the size range (**Figure S1B**). Titration of the cGAMP-VLP on THP-1 cells induced a dose-dependent upregulation of SIGLEC-1, an IFN-stimulated gene that is upregulated in response to STING activation (**Figure S1C**). Comparison to the clinically tested CDN ADU-S100 (2'3'-c-di-AM(PS)2(Rp,Rp)) *(3)* or to synthetic 2'3'-cGAMP demonstrated that cGAMP-VLP was ~500x and ~200x more effective at inducing SIGLEC-1, respectively. Even when intracellular delivery of ADU-S100 or 2'3'-cGAMP was enhanced using lipofectamine, cGAMP-VLP was still ~9x and ~50x more effective than the lipofected ADU-S100 or 2'3'-cGAMP, respectively.

Intra-tumoral injection of cGAMP-VLP induces tumor rejection

To assess the anti-tumor effect of cGAMP-VLP, we used male murine bladder tumor cell line MB49. MB49 cells implanted by the sub-cutaneous route induce a spontaneous immune response in female mice that leads to partial tumor regression mediated by T cells *(13)*. We initiated treatment on 50 mm^3 tumors and performed three intra-tumoral injections of cGAMP-VLP

containing 50 ng cGAMP or injections of PBS, every three days (**Figure S1D**). Tumors grew continuously in the PBS group, and a minority of mice (3/8) spontaneously eliminated the tumor (**Figure S1E**). In contrast, all mice treated with cGAMP-VLP (8/8) eradicated the tumor and cGAMP-VLP induced a statistically significant anti-tumor effect (**Figure S1F**). Measurement of the tumor-specific T cell response in the blood in some mice showed that cGAMP-VLP induced a significant increase in $CD4^+$ T cells responding to the tumor antigen DBy (**Figure S1G**). In addition, a fraction of mice treated with cGAMP-VLP showed a high level of $CD8^+$ T cell responses to the tumor antigen Uty.

Intra-tumoral injection of cGAMP-VLP induces T cell responses in a poorly immunogenic tumor model

This result suggested that cGAMP-VLP has the capacity to stimulate T cell responses against tumor antigens. To expand our analysis, we tested the effects of cGAMP-VLP in the murine tumor B16-OVA, which is poorly responsive to PD1 blockade *(14)*. We started treatment on palpable tumors and performed three intra-tumoral injections of either cGAMP-VLP, empty VLP (VLP), empty VLP with the matched dose of free 2'3'-cGAMP co-injected (VLP + equivalent cGAMP), free 2'3'-cGAMP alone, free ADU-S100 or PBS (**Figure 1A**). For cGAMP-VLP, we used an injection dose containing 33 ng of cGAMP in one experiment and 50 ng in a second experiment. For free 2'3'-cGAMP and ADU-S100, we used 50 µg per injection (1000-fold higher dose). To evaluate STING activation, we measured cytokines in the serum 3h after the first injection (**Figure 1B**). cGAMP-VLP, ADU-S100 and 2'3'-cGAMP induced IFN-α, IFN-β, IL-6 and TNF-α, while empty VLP did not induce these cytokines. cGAMP-VLP induced significantly more IFN-α, IFN-β and TNF-α than the VLP + equivalent cGAMP, consistent with the enhanced intra-cellular delivery of cGAMP contained in the VLP of cGAMP-VLP. Low (33 ng) or higher

doses (50 ng) cGAMP-VLP induced similar levels of cytokines compared to 50 µg free 2'3'-cGAMP. ADU-S100 (50 µg) induced higher levels of the cytokine, suggesting that STING stimulation across cell types was not saturated by cGAMP-VLP. These results show that cGAMP-VLP induces cytokine responses that require a 1000-fold less amount of cGAMP compared to the synthetic molecule.

We next measured tumor growth in mice treated with STING agonists. ADU-S100 and cGAMP-VLP were tested with or without anti-PD1 to assess the impact of immune checkpoint inhibition on the response. cGAMP-VLP induced a delay in tumor growth, while adding anti-PD1 enhanced this delay and led to complete responses in a subset of mice (**Figure 1C,D**). In comparison, ADU-S100 induced a delay in tumor progression and some complete responses, but there was no additive effect of anti-PD1. 2'3'-cGAMP alone or co-injected with VLP induced a smaller tumor growth delay and no complete responses were observed. Empty VLP had no effect. Similar trends were observed in mouse survival (defined in this study as the time until the ethical endpoint of 2000 mm^3 tumor size is reached) (**Figure 1E**). Specifically, anti-PD1 enhanced the survival of mice treated with cGAMP-VLP, while it had no impact when combined with ADU-S100. Furthermore, we observed that the anti-tumor effect of ADU-S100 was characterized by necrosis of all the injected tumors, while necrosis was rarely observed with cGAMP-VLP **(Figure S2A)**.

These results suggested potential differences in T cell responses induced by cGAMP-VLP compared to ADU-S100, leading us to measure the frequency of OVA-specific $CD4^+$ and $CD8^+$ T cell responses in blood 10 days after treatment initiation. cGAMP-VLP induced significant T cell responses and the majority of mice showed detectable responses (**Figure 1F**). In contrast, ADU-S100 did not induce detectable T cell responses in most mice. In the few mice that a T cell response was detected, its magnitude did not reach the average response observed with cGAMP-VLP. It has

been proposed that ADU-S100 ablates the T cell responses, and that at lower doses it may induce tumor-specific T cell responses in blood *(4)*. We thus performed a dose-titration of ADU-S100 in the B16-OVA model and observed a dose-response anti-tumor effect (**Figure S2B**). In the blood, we detected OVA-specific $CD8^+$ responses at the highest dose of ADU-S100 in a subset of mice, but these were not significant (**Figure S2C**). No OVA-specific $CD8^+$ response was observed at lower doses of ADU-S100, nor in $CD4^+$ T cells. Thus, lower doses of ADU-S100 do not induce tumor-specific T cell responses in blood in this model. We conclude that intra-tumoral injection of cGAMP-VLP stimulates immunogenic anti-tumor T cell responses at low doses of cGAMP.

Tumor specific T-cell responses elicited by intra-tumorally administered cGAMP-VLP translate into systemic synergy with anti-PD1

We next sought to explore whether the T cell responses induced by cGAMP-VLP translate into systemic anti-tumor effect. To this end, we used a B16-OVA dual tumor model in which STING agonists were injected into one tumor (**Figure 2A**). Intra-tumoral injection of cGAMP-VLP or ADU-S100 in one of the tumors induced IFN-α, IFN-β, IL-6 and TNF-α in the blood (**Figure 2B**). 10 days later, significant levels of OVA-specific $CD8^+$ and $CD4^+$ T cells were detected in the blood of cGAMP-VLP treated mice (**Figure 2C**). In contrast, ADU-S100 induced T cell responses only in a minority of mice that were not statistically significant compared to the control group. We next monitored tumor growth in groups co-treated or not with anti-PD1, which confirmed that B16-OVA was resistant to anti-PD1 (**Figure 2D).** cGAMP-VLP induced a delay in tumor growth in local and distant tumors, and addition of anti-PD1 extended the delay and increased the number of eradicated tumors (**Figure 2D**). In contrast ADU-S100 induced a strong anti-tumor effect that was characterized by necrosis at the injected tumor **(Figure S2D).** At the distal tumor, ADU-S100 induced an anti-tumoral effect, but this effect was not enhanced by anti-

PD1 (**Figure 2E**). Ultimately, cGAMP-VLP combined with anti-PD1 decreased the distal tumor size more potently than ADU-S100, irrespectively of its combination with anti-PD1 (**Figure 2F**). Completely responding mice were challenged at day 80 with a second round of tumor graft. Mice that eradicated their initial tumor following cGAMP-VLP treatment were more resistant to the formation of a new tumor than mice that received ADU-S100 (**Figure 2G**). We conclude that cGAMP-VLP demonstrated a synergistic effect with anti-PD1, enhancing the ability of B16-OVA bearing mice to respond to immune checkpoint blockade. In contrast, the synthetic CDN ADU-S100 induces systemic anti-tumor responses that do no elicit OVA-specific T cells response and do not synergize with anti-PD1.

cGAMP-VLP requires host STING and T cells to induce anti-tumor effects

To understand the nature of the anti-tumor response induced by cGAMP-VLP, we tested the role of STING and T cells using *Sting1* and *Rag2* knock-out mice, respectively (**Figure 3A**). We selected a dual tumor B16-OVA model treated with intra-tumoral 50 ng cGAMP-VLP or 50 µg ADU-S100 monotherapy. Induction of IFN-α, IL-6 and TNF-α by cGAMP-VLP or ADU-S100 was lost in *Sting1*$^{-/-}$ mice, indicating that STING is required in host cells (**Figure 3B**). In contrast, these cytokines were still induced in *Rag2*$^{-/-}$ mice showing that T cells were not required for generation of the early cytokine response. Next, we measured the OVA-specific $CD4^+$ and $CD8^+$ T cell response in blood. As expected, the T cell responses induced by cGAMP-VLP were not detected in *Rag2*$^{-/-}$ mice (**Figure 3C**). In *Sting1*$^{-/-}$ mice, T cell responses induced by cGAMP-VLP were heterogeneous and not statistically significant, as compared to WT mice. Nevertheless, T cell responses were detectable in some of the mice, indicating that additional pathways contribute to the immune-stimulating activity of cGAMP-VLP. Upon examining tumor growth, the anti-tumor effect of cGAMP-VLP and ADU-S100 on the size of injected and distal tumors was lost in *Sting1*$^{-}$

$^{-/-}$ (**Figure 3D**). In *Rag2*$^{-/-}$ mice, the anti-tumor effect cGAMP-VLP was lost in the injected and distal tumors. In contrast, the effect of ADU-S100 was maintained in the injected tumors, but lost at the distal ones. Consistently, cGAMP-VLP and ADU-S100 increased the survival of dual B16-OVA tumor bearing mice compared to PBS treated mice, and these increases were abolished in *Sting1*$^{-/-}$ or *Rag2*$^{-/-}$ mice (**Figure 3E**).

To assess the origin of the residual and variable T cell responses in *Sting1*$^{-/-}$ mice in response to cGAMP-VLP, we considered the role of STING in tumor cells. We generated *Sting1* knockout (KO) and control B16-OVA (**Figure S3A**). The induction of IFN-β and TNF-α was reduced in *Sting1* KO tumor cells implanted in WT mice, while they were not significantly induced in control tumor cells implanted in *Sting1* KO mice (**Figure S3B, S3C, S3D**). Similarly, the T cell responses and the anti-tumor effects induced by cGAMP-VLP were more impacted by *Sting1* KO in the host than *Sting1* KO in tumor cells (**Figure S3E, S3F**). Of note, residual anti-tumor activity of cGAMP-VLP was observed when *Sting1* was deleted in both tumor and host, despite the lack of detectable cytokine induction and of significant anti-tumor T cell responses in blood.

These results prompted us to test the relative role of $CD8^+$ T cells and NK cells in tumor elimination induced by cGAMP-VLP using depleting antibodies (**Figure S4A**). The anti-CD8α antibody induced a depletion of $CD8^+$ T cells at day 7 and 17, an increase in NK cells at day 17, and no effect on $CD4^+$ T cells (**Figure S4B**). In contrast the anti-NK1.1 antibody depleted NK cells and had a slight depleting effect on $CD8^+$ T cells at days 7. The antibodies had no effect on cytokine production induced by cGAMP-VLP at day 7, two days after the first round of depletion (**Figure S4C**). As expected, the anti-CD8α antibody blunted the detection of OVA-specific $CD8^+$ T cells (**Figure S4D**). $CD8^+$ T cell depletion also eliminated the effect of cGAMP-VLP on mouse survival, while NK cell depletion had no effect (**Figure S4E**). We conclude that the anti-tumor effect of

cGAMP-VLP requires STING in the host and the presence of $CD8^+$ T cells, but not NK cells, while the effect of ADU-S100 requires host STING but is partially independent of T cells.

Immune cell composition and activation differentiates cGAMP-VLP from ADU-S100

Our results thus far showed that while high levels of tumor-antigen-specific T cells were detected in the blood of cGAMP-VLP treated mice but not in ADU-S100 treated mice, the abscopal anti-tumoral effect of both treatments required T cells. To resolve this paradox, we investigated the composition and activation status of immune cells in tumors and lymphoid organs (**Figure 4A**). In the injected tumors, cGAMP-VLP induced an increase in $CD8^+$ T cells and a decrease in $CD4^+$ Tregs and NK cells (**Figure 4B, top panel**). In contrast, ADU-S100 depleted $CD45^+$ cells, in particular NK and $CD4^+$ T cells, while ADU-S100 had no impact on $CD8^+$ T cells or Tregs. In the distal tumor, cGAMP-VLP induced an increase in $CD8^+$ T cells but Tregs levels were not affected (**Figure 4B, bottom panel**). In contrast, ADU-S100 had no significant impact on the proportion of immune cells based on the markers tested in the distal tumor. We next analyzed lymphoid organs. In the tumor-draining lymph nodes, cGAMP-VLP increased the proportion of effector memory $CD4^+$ and $CD8^+$ T cells (**Figure 4C, left panel**). In contrast, ADU-S100 decreased the frequency of central memory $CD4^+$ T cells, had no impact on effector memory $CD4^+$ T cells, and increased the proportion of effector memory $CD8^+$ T cells. In non-draining lymph nodes and in the spleen, both cGAMP-VLP and ADU-S100 increased the proportion of effect memory $CD8^+$ T cells (**Figure 4C, middle and right panels**). Surprisingly, both cGAMP-VLP and ADU-S100 increased effector memory $CD8^+$ T cells in all lymphoid organs examined, but only cGAMP-VLP induced robust levels of tumor antigen-specific T cell responses. This raised the possibility that ADU-S100 might induce T cell activation independently from tumor antigens. To test this possibility, we examined the level of CD69, an early marker of T cell activation. Strikingly, ADU-S100 induced

upregulation of CD69 in tumors and in all lymphoid organs tested, in both $CD4^+$ and $CD8^+$ (**Figure 4D**). This reached up to 20% and 30% of T cells in spleen and non-draining lymph nodes, a week after the last injection of ADU-S100. This systemic effect was not observed with cGAMP-VLP, which induced significant levels of CD69 in non-draining lymph nodes, but not in other organs tested. This result suggests that ADU-S100 induces a general activation of T cells, which does not appear to translate into the systemic expansion of tumor antigen-specific T cells, while cGAMP-VLP appears to induce a specific and systemic T cell response for tumor antigens.

cGAMP-VLP targets preferentially antigen-presenting cells

To understand the induction of tumor antigen-specific T cells by cGAMP-VLP, we analyzed its effect *in vitro* on a set of cell types present in the tumor micro-environment, starting with cell lines. We treated the tumor cell line B16-OVA, the endothelial cell line MS1, the dendritic cell line MutuDC and the macrophage cell line RAW 264.7 (RAW hereafter). cGAMP-VLP induced the highest levels of IFN-β in RAW cells, followed by MutuDC and MS1, in a dose-dependent manner (**Figure S5A, S5B**). The IFN-β induction in B16-OVA cells was the lowest. ADU-S100 also induced dose-dependent IFN-β, but was less cell-type selective than cGAMP-VLP. Soluble cGAMP induced detectable IFN-β only at the highest tested dose.

To gain further insights in the induction of interferons by antigen-presenting cells, we treated bone marrow derived macrophage (BMDM) and dendritic cells (BMDC). The latter obtained either with GM-CSF, which generates mainly inflammatory dendritic cells, or with FLT3L, which generates a mixed population of type 1 conventional dendritic cells (cDC1), type 2 cDC (cDC2), and plasmacytoid dendritic cells. cGAMP-VLP and ADU-S100 induced similar levels of IFN-α and IFN-β in BMDM and BMDC (with GM-CSF) (**Figure S5C**). In contrast, cGAMP-VLP induced significantly higher levels of both cytokines in BMDC (with FLT3L)

(**Figure S5D**). Synthetic cGAMP induced detectable cytokines only at the highest tested dose, despite 1000-fold higher amounts than in cGAMP-VLP. These results suggested a preferential activation of STING in antigen-presenting cells by cGAMP-VLP, in particular in FLT3L-derived cells. To determine if this effect was associated with preferential uptake of the particles, we attempted to detect cGAMP-VLP *in vivo* in samples stained for p24, but the antibody-based detection was not sensitive enough. As a surrogate, we treated splenocytes with cGAMP-VLP and stained for p24 (**Figure S6A**). The highest levels of uptake were detected in macrophages, cDC1 and cDC2 (**Figure S6B, S6C, S6D**). The particles were also detected in some lymphocytes, but only in a fraction of cells within each population. Altogether these results indicate that cGAMP-VLP targets preferentially antigen-presenting cells.

STING is required in dendritic cells for T cell-mediated anti-tumor effects of cGAMP-VLP

To decipher the contribution of STING within antigen-presenting cells, we generated STING-OST^{fl} mice in which the first coding exon of *Sting1* was flanked by LoxP sites. We also introduced a Twin-Strep-tag (OST) at the N-terminus of STING protein. We crossed the mice to *LysM-cre* (STING-OST$^{\Delta LysM}$) or *Itgax-cre* (STING-OST$^{\Delta Cd11c}$) and confirmed preferential deletion of STING in splenic macrophages or dendritic cells, respectively (**Figure S7A, S7B**). In STING-OST$^{\Delta LysM}$ mice, IFN-α and IL-6 in serum were not significantly induced by cGAMP-VLP and ADU-S100 in comparison to the PBS-treated group (**Figure 5B**). However, the induction of OVA-specific T cells by cGAMP-VLP and the anti-tumoral effect were maintained in STING-OST$^{\Delta LysM}$ mice (**Figure 5C,D**). In comparison, the anti-tumor effect of ADU-S100 was reduced on the distal tumor in STING-OST$^{\Delta LysM}$ compared to STING-OST^{fl} controls (**Figure 5D**). In STING-OST$^{\Delta Cd11c}$ mice, IFN-α and IL-6 were not significantly induced by cGAMP-VLP, while ADU-S100 induced significant levels of the cytokines, compared to PBS treatment in STING-OST$^{\Delta Cd11c}$ mice. (**Figure**

5E). In contrast to STING-OST^{fl} mice, cGAMP-VLP did not induce significant levels of OVA-specific T cells in STING-OST$^{\Delta Cd11c}$ mice, although responses were still detected in some mice compared to the PBS group (**Figure 5F**). The anti-tumor effect of both ADU-S100 and cGAMP-VLP was reduced on the distal tumor in STING-OST$^{\Delta Cd11c}$ compared to STING-OST^{fl} mice (**Figure 5G**). Of note, ADU-S100 induced detectable OVA-specific T cell responses in some OST-STING^{fl} mice (**Figure 5C,F**), that were not observed in WT mice (**Figure 3C**). Importantly, CD11c is expressed on tumor macrophages notably in the B16 tumor model *(15)*. Therefore, these results indicate that STING is specifically required in dendritic cells for the distal anti-tumor effect of cGAMP-VLP, while the distal anti-tumor effect of ADU-S100 depends on STING in macrophages or dendritic cells.

cDC1 are required for T-cell mediated anti-tumor activity of STING stimulation

To further address the role of dendritic cells in the anti-tumoral activity of cGAMP-VLP and ADU-S100, we analyzed the proportion of the main DC subsets, cDC1 and cDC2, and the expression of their activation markers CD80 and CD86, in tumor, draining lymph node and spleen, one day after treatment (**Figure 6A**). In tumors, we found that cDC1 became undetectable in ADU-S100 treatment tumors (**Figure 6B, 6C**). cDC2 were also substantially reduced and not activated based on their low expression of CD80 and CD86. In contrast, cGAMP-VLP treatment induced a milder decrease of cDC1 and cDC2, and cDC1 upregulated CD86 (**Figure 6C**). In draining lymph node, cDC1 and cDC2 were detected and upregulated CD80 and CD86 in response to ADU-S100, and CD86 in response to cGAMP-VLP (**Figure S7C**). In spleen, ADU-S100 decreased cDC1, as observed in tumors (**Figure S7C**). CD86 was induced in splenic cDC1 and cDC2 in response to ADU-S100 and cGAMP-VLP (**Figure S7C**). Altogether, these results show that while dendritic

cells get activated in response to ADU-S100 and cGAMP-VLP, ADU-S100 depletes cDC1 in multiple locations.

Since cDC1 are required for cross-presentation of tumor antigen in other settings, these results suggested that cDC1 may be engaged by cGAMP-VLP. To address this question, we used the *Xcr1*^{DTA} model that lacks cDC1 constitutively *(16)* (**Figure 6D**). In *Xcr1*^{DTA}, the induction of OVA-specific CD8^{+} T cells by cGAMP-VLP was abrogated (**Figure 6E**). The induction of OVA-specific CD4^{+} T cells was also reduced on average, but this was not statistically significant. Accordingly, the anti-tumor activity of cGAMP-VLP was lost in *Xcr1*^{DTA} (**Figure 6F**). In contrast, ADU-S100 maintained its anti-tumoral activity in absence of cDC1. We conclude STING stimulation with ADU-S100 depletes cDC1, while STING stimulation with cGAMP-VLP depends on cDC1 for anti-tumor activity.

Systemic administration of cGAMP-VLP activates anti-tumor T cells immunity

The activation of STING in dendritic cells by cGAMP-VLP and the implication of cDC1 that mediate tumor antigen cross-presentation raised the possibility that STING stimulation by cGAMP-VLP could induce anti-tumor T cell responses even after injection outside of the tumor mass, in proximity to tumor-draining lymph nodes that spontaneously receive antigens from tumors *(17)*. We first tested sub-cutaneous (s.c.) injection of cGAMP-VLP in the B16-OVA model in combination with anti-PD1 (**Figure 7A**). S.c. injection of cGAMP-VLP induced detectable levels of IFN-α, IFN-β, IL-6 and TNF-α, albeit to lower levels than following intra-tumoral (i.t.) injection (**Figure 7B**). Tumor growth was delayed after s.c. injection of cGAMP-VLP (**Figure 7C**), leading to significantly smaller tumors (**Figure 7D**). cGAMP-VLP s.c. also induced anti-OVA T cell responses (**Figure 7E**) and increased the survival of tumor-bearing mice, albeit not to the same level as i.t. cGAMP-VLP (**Figure 7F**).

In these experiments, the i.t. route remained more effective than the s.c. route at inducing T cell responses and anti-tumor effects, suggesting that a negative regulator of the immune response might be eliminated locally by i.t. activation of STING. We previously noted that cGAMP-VLP induced a reduction of Tregs in the injected tumor, but not in the distal tumors (**Figure 4B**). This raised the possibility that intra-tumoral Tregs might limit the anti-tumor effect of systemic STING activation by cGAMP. In order to test this hypothesis, we used an IgG2a isotype antibody against CTLA4 (anti-CTLA4-m2a), which has been shown to selectively deplete Tregs in tumors *(18, 19)*, and we confirmed this effect in the MCA-OVA tumor model (**Figure 7G, 7H**). Treatment with anti-CTLA4-m2a had no effect on the induction IFN-α, IL-6 and TNF-α by cGAMP-VLP (**Figure S8A**). In monotherapy, cGAMP-VLP s.c. or anti-CTLA4-m2a increased the frequency of OVA-specific $CD8^+$ and $CD4^+$ T cells, but no significant response to the endogenous tumor antigen p15 (**Figure 7I, S8B**). In contrast, combining cGAMP-VLP s.c. with anti-CTLA4-m2a synergized to significantly increase the levels of T cells against p15, and further increased the levels of T cells reactive to OVA. Accordingly, combination therapy induced a near-complete reduction in tumor size (**Figure 7J, S8C**). Similarly, monotherapies induced an increase in survival, but only the combination therapy induced long-term survival of treated mice (**Figure 7K**). Completely responding mice were also protected from a secondary tumor challenge (**Figure S8D**). To evaluate this synergy in another model, we used the aggressive B16-F10 model. The combination of cGAMP-VLP and anti-CTLA4-m2a extended the survival of treated mice, while the monotherapy with either compound showed no survival benefit in this model (**Figure S8E**).

To determine if STING stimulation by cGAMP-VLP was active in spontaneous tumors, we used the MMTV-PyMT model which produces one to several breast tumors per mouse. This model has been reported to be resistant to anti-PD1 *(20)*, and we showed above that the tumor-specific T cells induced by cGAMP-VLP respond to anti-PD1. Therefore, we included anti-PD1 as a baseline

treatment (**Figure 8A**). Injection with cGAMP-VLP significantly decreased tumor growth (summing the size of all tumors per mouse) and extended survival (**Figure 8B,C**). We conclude that systemic administration of cGAMP-VLP activates anti-tumor T cell immunity that synergizes with tumor Treg depletion and is active against spontaneous tumors.

Differential response to cGAMP-VLP vs ADU-S100 in human tumor samples

We next sought to determine if the differential impact of cGAMP-VLP and ADU-S100 on dendritic cells was maintained in human tumor samples. We previously showed that cGAMP-VLP efficiently activates STING in human dendritic cells *(11)*. We obtained two matched tumor and lymph node samples from head and neck cancer patients, and treated them ex vivo with cGAMP-VLP or ADU-S100 (**Figure 8D**). In the tumor samples, ADU-S100, but not cGAMP-VLP, depleted live dendritic cells, mirroring our findings in mice (**Figure 8E**). In lymph node samples, we observed that cGAMP-VLP, but not ADU-S100, increased the expression level of PDL1 and CD83 in dendritic cells (**Figure 8F, S9A**). ADU-S100 induced a stronger cytokine response than cGAMP-VLP at the doses used in both tumor and lymph node samples, indicating that the reduced activation of dendritic cells was not due to lack of STING activation overall (**Figure S9B**). We conclude that the differential immunostimulatory activity of cGAMP-VLP and ADU-S100 is likely conserved between humans and mice.

Discussion

Overall, our results establish that cell targeting of STING stimulation towards dendritic cells promotes anti-tumor T cell responses against tumor antigens. We found that cGAMP delivery by virus-like particles preferentially activates STING in dendritic cells compared to the synthetic STING agonist ADU-S100, and at lower effective doses of STING ligand. cGAMP-VLP activates systemic T cell responses that induce synergistic anti-tumor responses with PD1 blockade or tumor Treg depletion. In contrast, despite its potent local anti-tumor effect, the synthetic STING agonist inefficiently induces systemic anti-tumor T cell responses. Mechanistically, the systemic anti-tumor effect of cGAMP-VLP relies on cDC1 and STING expression in dendritic cells, while ADU-S100 depletes immune cells in particular cDC1.

These results highlight the crucial importance of targeting STING activation in specific cell types, particularly dendritic cells, to optimize the antigen-specific anti-tumor responses. STING was previously shown to be required in dendritic cells *in vitro* to induce an interferon response to immunogenic tumor cells or tumor DNA *(2, 21)*. *In vivo*, dendritic cells were found to be a major source of IFN-β in tumors that induce STING-dependent immunogenic responses *(22)*. Intriguingly, STING in $Cd11c^{+}$ cells was also implicated in the negative regulation of allogeneic immune responses *(23)*. Altogether, STING activation in dendritic cells has emerged as a key component for the induction of antigen-specific T cell responses.

In contrast to cGAMP-VLP, the anti-tumor responses induced by ADU-S100 were not associated with the induction of tumor-specific T cells. While it was previously proposed that the induction of antigen-specific T cells by ADU-S100 was dose-dependent *(4)*, we did not observe such bimodal behavior in the tumor model we tested. We do not exclude the possibility that ADU-S100 might produce tumor-specific T cell responses in the injected tumor, but if such induction occurs, it does not appear to be sufficient to induce detectable tumor-specific T cells in peripheral

blood using our assays, while cGAMP-VLP robustly induced circulating anti-tumor T cell responses. We noted that ADU-S100 induced some level of tumor-specific T cells in experiments with OST-STING^{fl} mice bred in-house (**Figures 5C, 5F**), but not with mice obtained from an external source (**Figures 1F, 2C, S2C**). This raises the intriguing possibility that housing parameters, such as the composition of the microbiota, or the presence of the OST tag on STING, might affect the immunogenic properties of synthetic CDNs. We also noted that synthetic CDNs induced necrosis at the intra-tumoral injection site which was rarely observed with cGAMP-VLP. This is consistent with a role of STING activation in endothelial cells caused by synthetic CDNs as contributing to its local anti-tumor effects *(24–26)*. The reduced dose of cGAMP in cGAMP-VLP compared to free CDN likely contributes to the reduced tissue necrosis after cGAMP-VLP treatment.

Multiple approaches have been proposed to optimize delivery of CDNs for use as immunomodulators in the absence of exogenous tumor antigens. Synthetic nanoparticles have been shown to enhance cytosolic delivery of CDNs and activate STING-dependent anti-tumor responses *(27, 28)*. Exosomes loaded with CDNs appear to achieve similar enhancements *(29, 30)*. Principles to ensure that delivery with synthetic approaches will yield tumor-specific T cell responses generated are currently poorly defined. A common limitation of synthetic cargos and exosomes lies in the passive delivery mechanism to target cells. In contrast, cGAMP-VLPs employ a viral fusion glycoprotein to efficiently fuse with target cells. The size of the VLPs, their lipid bilayer originating from a producer cell and the fusion triggered by VSV-G in acidic endosomes most likely contribute to the selectivity of cGAMP-VLPs for antigen-presenting cells, in particular dendritic cells. Accordingly, retroviral particles are also efficiently captured by antigen-presenting cells *in vivo (31)*. In addition, a higher expression of STING or downstream signaling proteins in antigen-presenting cells might also contribute to their selectivity.

The anti-tumor efficacy of cGAMP-VLP requires STING expression in the host. Using the intra-tumoral route of injection, optimal efficacy also implicates STING expression in tumor cells, but this is not essential. Residual levels of anti-tumor $CD8^+$ T cells and anti-tumor activity of cGAMP-VLP remained detectable in STING knockout mice grafted with STING knockout tumor cells, suggesting that cGAMP-VLP targets additional innate immune pathways. Beyond STING, additional putative targets of cGAMP have been proposed *(32, 33)*, but the immunomodulatory effect of these targets is not known. Additionally, virus-like particles have recently been reported to prime RIG-I-like receptors *(34)*. The existence of additional modes of action of cGAMP-VLP, and in particular of cGAMP, warrants further investigation.

We found that the optimal induction of anti-tumor T cells and the distal anti-tumor effect of cGAMP-VLP required STING expression in Cd11c-expressing cells but not LysM-expressing cells, indicating a requirement of STING in dendritic cells. However, we do not exclude a residual contribution from tumor-associated macrophages that is not fully eliminated by LysM-cre, notably in the case of the intra-tumoral route of administration of cGAMP-VLP. Analysis of dendritic cells early after treatment demonstrated that ADU-S100 reduces cDC2 levels and essentially eliminates cDC1 from the injection site. Accordingly, genetic elimination of cDC1 using $Xcr1^{DTA}$ mice also inhibited the induction of anti-tumor tumor T cells by cGAMP-VLP and its anti-tumoral activity. A limitation of our study is that selective deletion of STING in cDC1 by breeding to Xcr1-cre mice was not possible due to an unmanageable level of germline deletions in this model, as shown previously in two studies *(16, 35)*. Nonetheless, we observed that ADU-S100 also depleted dendritic cells in human head and neck cancer samples. The elimination of dendritic cells by ADU-S100, and presumably related synthetic compounds, will likely limit their immunogenic activity in humans and their ability to provide benefits in combination with inhibitors of T cell checkpoints. The ability to preserve dendritic cell viability while promoting their activation was also proposed

in the context of inflammasome stimulation *(36)* and, therefore, emerges as an important factor for the success of immunotherapies that aim at priming anti-tumor T cells.

Altogether, our results establish that cell type-specific activation of STING plays a critical role in anti-tumor immunogenicity. Synthetic STING agonists appear to induce promiscuous STING activation that does not necessarily entail priming of tumor-specific T cells. In contrast, cGAMP-VLP constitutes a biological product that activates STING preferentially in dendritic cells, leading to activation of tumor-specific T cells, which synergize with ICB and Treg depletion. Biological stimulation of STING with cGAMP-VLP has the potential, similar to other biologics such as antibodies and CAR-T cells, to contribute to a meaningful treatment regimen to improve anti-tumor immune responses in patients.

Materials and Methods

Study design

The study was designed to evaluate the anti-tumor activity and the mechanism of activation of cGAMP-VLP. ADU-S100 was used as a treatment of reference. The goal of the study was to evaluate the activation of STING signaling, the induction of systemic anti-tumor T cells and the anti-tumor activity of the compounds in various tumor models in mice and humans, in monotherapy or in combination with reference antibody-based immunotherapies. Mechanistically, the goal of the study was to determine the cell targeting provided by virus-like particles, the contribution of STING among cell types and the role of specific immune cell populations in the anti-tumor effects. Mice of different genotypes were used. Baseline differences were often observed between genotypes in the PBS treatment group. Therefore, comparisons between treatments were made, in general, to the PBS control within the same genotype. Ethically approved humane endpoints were followed to terminate in vivo experiments with tumor-bearing mice. Tumor-bearing mice were randomized using RandMice (https://randmice.com) based on tumor volume to distribute mice and homogenize the average tumor volume within the different groups. The algorithm randomly shuffles all mice between the groups and calculates the average tumor volume for each group. 10^9 iterations are performed in order to minimize the difference in tumor volume average between all groups. The study was not blinded. The number of samples combined and the number of independent experiments are included in the figure legends.

Cell culture

Cell lines used in the study are listed in Table S1. 293T cells, RAW 264.7 cells and MS1 cells were cultured in DMEM GlutMAX, 10% fetal bovine serum (FBS) (Gibco), and penicillin-streptomycin (Gibco). THP-1 cells were cultured in RPMI GlutMAX medium, 10% FBS (Gibco), and penicillin-

streptomycin (Gibco). B16-OVA cells were cultured in RPMI GlutMAX medium with 10% FBS (Gibco), penicillin-streptomycin (Gibco), 1 mM 2-mercaptoethanol, geneticin and hygromycin. MCA-OVA cells were cultured in RPMI GlutMAX medium with 10% FBS (Gibco), penicillin-streptomycin (Gibco), 1 mM 2-mercaptoethanol, and hygromycin. MB49 cells were cultured in DMEM GlutMAX medium with 10% FBS (Gibco) and penicillin-streptomycin (Gibco). B16-F10 cells were cultured in DMEM medium with 10% FBS. MutuDC were cultured as described *(37)*. The splenocytes were culture in RPMI GlutMAX with 10% FBS (Gibco), penicillin-streptomycin (Gibco), 1 mM 2-mercaptoethanol.

Plasmids, proteins and peptides.

Plasmids, proteins and peptides used in the study are listed in Table S2. pLentiCRISPRv2-mSTING-gRNA_1 (GCTGGATGCAGGTTGGAGTA), pLentiCRISPRv2-mSTING-gRNA_2 (AGCGGTGACCTCTGGGCCGT), pLentiCRISPRv2-mSTING-scrambled_gRNA_1 (CTTTGCGGAGATTGGAGGGA) and pLentiCRISPRv2-mSTING-scrambled_gRNA_2 (GCCGTTGCCGACGGTACGTG) were cloned in lentiCRISPRv2. psPAX2 have been previously described *(11)*. pVAX1-cGAS was obtained by cloning codon-optimized human cGAS in pVAX1. pVAX1-VSVG-INDIANA2 was obtained by cloning the VSV-G coding sequence and flanking non-coding sequences from pCMV-VSV-G in pVAX1.

Generation of STING knockout and control B16-OVA cells.

Control and *Sting1* KO B16-OVA cells were obtained by transducing B16-OVA with the corresponding lentivectors prepared using standard methods. Cells were selected for one week with 2 mg/mL of Puromycin (Invivogen). Knock-out efficiency was measured by western blotting.

Antibodies.

References for antibodies are listed in Table S3.

cGAMP-VLP production for *in vivo* use

7.5 million 293T cells were plated in 150 cm² cell culture flask and incubated overnight. One batch of cGAMP-VLP was made from 4 flasks. The following day, each flask was transfected with 13 µg of pVAX1-cGAS, 8.1 µg of HIV-1 psPAX2, 3.3 µg of pVAX1-VSVG-INDIANA2, and 50 µL of PEIpro, according to the manufacturer's instructions. The transfection mixes were prepared in Opti-MEM (Gibco). The morning following transfection, the medium was changed with 52 mL of warm VLP production medium (293T culture medium with 10 mM HEPES and 50 µg/mL Gentamicin). One day later, the cGAMP-VLP-containing supernatant was harvested from the cells, centrifuged for 10 minutes at 200 *x g* 4°C, and filtered through 0.45 µm nylon mesh filters (Fisher 22363547). 39 mL of cGAMP-VLP-containing supernatant was gently overlaid on 6 mL of cold PBS containing 20% sterile filtered endotoxin free sucrose in 6 Ultra-Clear tubes (Beckman Coulter, ref 344058), and centrifuged for 1 hour and 30 minutes at 100,000 *x g* 4°C. The liquid phase was gently aspirated, the pellets were resuspended in cold PBS and transferred to one Ultra-Clear 13.2 mL tube (Beckman Coulter, ref 344059) and centrifuged again at 100,000 *x g* 4°C for 1 hour and 30 minutes. The PBS was gently poured out and the pellet was resuspended in 320 µL of cold PBS. Batches were split in 3 aliquotes of 100 µL for experimental use. The remaining 20 µL were diluted 1:4 with 60 µL of PBS and split in 8 aliquotes of 10 µL for quality control assays. Aliquotes were stored at -80°C.

cGAMP quantification

Commercial assays used in the study are listed in Table S4. 2'3'-cGAMP ELISA Kit (Cayman Chemical) was used for the quantification of cGAMP in cGAMP-VLP according to the manufacturer's instructions. After performing the assay, the plate was read at a wavelength of 450 nm. Data was fitted to a 4-parameter sigmoidal curve.

Biological activity assay of cGAMP-VLP

50,000 THP-1 cells were plated in round bottom 96 well plates in 100 µL of medium, and stimulated with serial-dilutions of cGAMP-VLP, soluble cGAMP or soluble ADU-S100 in 100 µL. Where indicated, CDN (6 µg) were mixed with lipofectamine 2000 (6 µL) in Opti-MEM (12.75 µL each) following manufacturer's instructions. The cells were incubated for 18 to 24 hours and stained with an anti-human SIGLEC-1, fixed in PFA 1% and acquired using a BD FACSVerse cytometer.

Electron microscopy

cGAMP-VLP suspension was deposited on formvar/carbon–coated copper/palladium grids before uranyl/acetate contrasting and methyl-cellulose embedding for whole-mount. Images were acquired with a digital camera Quemesa (EMSIS GmbH, Münster, Germany) mounted on a Tecnai Spirit transmission electron microscope (FEI Company) operated at 80 kV.

Nanoparticle Tracking Analysis

The cGAMP-VLP were serially diluted in PBS at room temperature and acquired on a NanoSight as previously described *(38)*.

Mice

All animals were used according to protocols approved by Animal Committee of Curie Institute CEEA-IC #118 and maintained in pathogen-free conditions in a barrier facility. Experimental procedures were approved by the Ministère de l'enseignement supérieur, de la recherche et de l'innovation (APAFIS#11561-2017092811134940-v2) in compliance with the international guidelines. C57BL/6J female mice (6-8 weeks) were purchased from Charles River Laboratories. C57BL/6J *Rag2*$^{tm1.1Cgn}$ (*Rag2*$^{-/-}$) female mice (13-24 weeks) were maintained at Centre d'Exploration et de Recherche Fonctionnelle Expérimentale. C57BL/6J *Xcr1*^{DTA} male mice (5-12 weeks) were maintained at CIPHE pathogen-free animal facility. C57BL/6J *Lyz2*$^{tm1(cre)Ifo}$ (LysM-cre) mice, C57BL/6J Tg(Itgax-cre)1-1Reiz (Cd11c-cre) mice, C57BL/6J *Sting*$^{gt/gt}$ (*Sting1*$^{-/-}$) female mice (16-35 weeks), STING-OST^{fl} mice and MMTV-PyMT$^{+/-}$ female mice (20-21 weeks) were maintained at Institut Curie Specific Pathogen Free facility. For STING-OST^{fl} mice, experiments were performed with a mix of female and male mice from age 8 to 44 weeks. The experiments with B16-F10 tumors was performed at Crown Bioscience. Mice were allowed to acclimate to the experimental housing facility for at least three days before tumor injections.

Tumor implantation

Female or male mice were inoculated subcutaneously on the lower right or right and left flanks with either 5x10^5 B16-OVA cells in 100 µL of HBSS, or with 1x10^6 B16-OVA WT or *Sting1* KO cells in 100 µL of HBSS, or with 5x10^5 MB49 cells in 100 µL of PBS, or with 5x10^5 MCA-OVA cells in 100 µL of PBS, or with 2x10^5 B16-F10 cells in 100 µL of PBS. Mice were monitored for morbidity and mortality daily. Tumors were monitored twice or three times per week. Mice were euthanized if ulceration occurred or when tumor volume reached 2000 mm^3. Tumor sizes were measured using a digital caliper and tumor volumes calculated with the formula (length x width^2)/2. Following tumor implantation, mice were randomized into treatment groups using the Randmice

software. In some experiments, tumor-free survivors were challenged with tumor cells on the opposite, non-injected flank several weeks after the collapse of the primary tumor. Naive mice of the same age were used as controls.

In vivo immunotherapy

Intra-tumoral (i.t.) or subcutaneous (s.c.) injections were initiated when tumors are palpable or reached close to 50 mm^3 (40-80 mm^3) or when mean tumor size reached approximately 100 mm^3 (70-150 mm^3), as indicated in legends. A U-100 insulin syringe or equivalent [0.33 mm (29 G) x 12.7 mm (0.5 mL)] was filled with 50 µL of samples (VLP, cGAMP-VLP or synthetic CDN diluted in PBS) and all air bubbles were removed. Mice were anesthetized with isoflurane. With the bevel facing the skin, the needle was injected shallowly into the area directly adjacent to the tumor, and the needle was moved underneath the skin until it reached the inside back of the tumor. The samples were injected slowly into the center of the tumor (for the i.t.) or under the skin, 1 cm from the border of the tumor (for the s.c.). The needle was then removed delicately to avoid reflux. Treatments consisting of 200 µg of αPD1 antibody or 200 µg of isotype control antibody were diluted in PBS at 1 mg/mL and administered by intra-peritoneal (i.p.) injection at the indicated time points.

cGAMP-VLP capture by splenocytes *in vitro*

Spleens were harvested from female C57BL6/J mice. Splenocytes were isolated by pressing the organ through a 40 µm cell strainer. Red blood cells were lysed using an ammonium chloride lysis buffer as described above. 1 to 3 million cells were plated in a 96-well round bottom plate in 150 µL of medium. 50µL of cGAMP-VLP or PBS was added and cells were incubated overnight at 37°C 5% CO_2. The following day the cells were stained with antibodies against extracellular

markers (MHC-II eFluor450, CD4 BV785, NK1.1 PerCP-Cy5.5, CD11b PE, CD11c PETR, CD19 PE-Cy5, TCR-β PE-Cy7, CD8 APC, F4/80 AF700, Fixable Viability Dye eFluor780), washed and permeabilized using the BD Cytofix/Cytoperm Fixation Permeabilization Solution kit (reference 554714) according to the manufacturer's instructions. The cells were then washed with the permeabilization buffer, following by staining for 15 minutes at room temperature with a 1:100 dilution of a fluorescent anti-HIV-1 GAG antibody (KC57-FITC) in permeabilization buffer. Cells were washed, resuspended in FACS buffer and acquired on a Beckman Coulter CytoFlex S analyzer. The data was analyzed using FlowJo 10.

Design and Statistical Analysis

Statistical details of experiments are indicated in the figure legends, text or methods. Supplementary statistical tests cGAMP-VLP and ADU-S100 groups are listed in Data File S1. Data were analyzed in GraphPad Prism 8 software. In Figures, * $P < 0.05$, ** $P < 0.01$, *** $P < 0.001$, **** $P < 0.0001$.

List of Supplementary Materials

References

1. P. C. Tumeh, C. L. Harview, J. H. Yearley, I. P. Shintaku, E. J. M. Taylor, L. Robert, B. Chmielowski, M. Spasic, G. Henry, V. Ciobanu, A. N. West, M. Carmona, C. Kivork, E. Seja, G. Cherry, A. J. Gutierrez, T. R. Grogan, C. Mateus, G. Tomasic, J. A. Glaspy, R. O. Emerson, H. Robins, R. H. Pierce, D. A. Elashoff, C. Robert, A. Ribas, PD-1 blockade induces responses by inhibiting adaptive immune resistance. *Nature* **515**, 568–571 (2014).

2. S. R. Woo, M. B. Fuertes, L. Corrales, S. Spranger, M. J. Furdyna, M. Y. Leung, R. Duggan, Y. Wang, G. N. Barber, K. A. Fitzgerald, M. L. Alegre, T. F. Gajewski, STING-dependent cytosolic DNA sensing mediates innate immune recognition of immunogenic tumors. *Immunity* **41**, 830–42 (2014).

3. L. Corrales, L. H. Glickman, S. M. McWhirter, D. B. Kanne, K. E. Sivick, G. E. Katibah, S. R. Woo, E. Lemmens, T. Banda, J. J. Leong, K. Metchette, T. W. Dubensky Jr., T. F. Gajewski, Direct Activation of STING in the Tumor Microenvironment Leads to Potent and Systemic Tumor Regression and Immunity. *Cell Rep* **11**, 1018–30 (2015).

4. K. E. Sivick, A. L. Desbien, L. H. Glickman, G. L. Reiner, L. Corrales, N. H. Surh, T. E. Hudson, U. T. Vu, B. J. Francica, T. Banda, G. E. Katibah, D. B. Kanne, J. J. Leong, K. Metchette, J. R. Bruml, C. O. Ndubaku, J. M. McKenna, Y. Feng, L. Zheng, S. L. Bender, C. Y. Cho, M. L. Leong, A. van Elsas, T. W. Dubensky Jr., S. M. McWhirter, Magnitude of Therapeutic STING Activation Determines CD8(+) T Cell-Mediated Anti-tumor Immunity. *Cell Rep* **25**, 3074-3085 e5 (2018).

5. Y. Liu, A. A. Jesus, B. Marrero, D. Yang, S. E. Ramsey, G. A. Montealegre Sanchez, K. Tenbrock, H. Wittkowski, O. Y. Jones, H. S. Kuehn, C. C. Lee, M. A. DiMattia, E. W. Cowen, B. Gonzalez, I. Palmer, J. J. DiGiovanna, A. Biancotto, H. Kim, W. L. Tsai, A. M. Trier, Y. Huang, D. L. Stone, S. Hill, H. J. Kim, C. St Hilaire, S. Gurprasad, N. Plass, D. Chapelle, I. Horkayne-Szakaly, D. Foell, A. Barysenka, F. Candotti, S. M. Holland, J. D. Hughes, H. Mehmet, A. C. Issekutz, M. Raffeld, J. McElwee, J. R. Fontana, C. P. Minniti, S. Moir, D. L. Kastner, M. Gadina, A. C. Steven, P. T. Wingfield, S. R. Brooks, S. D. Rosenzweig, T. A. Fleisher, Z. Deng, M. Boehm, A. S. Paller, R. Goldbach-Mansky, Activated STING in a vascular and pulmonary syndrome. *N Engl J Med* **371**, 507–18 (2014).

6. S. Cerboni, N. Jeremiah, M. Gentili, U. Gehrmann, C. Conrad, M. C. Stolzenberg, C. Picard, B. Neven, A. Fischer, S. Amigorena, F. Rieux-Laucat, N. Manel, Intrinsic antiproliferative activity of the innate sensor STING in T lymphocytes. *J Exp Med* (2017), doi:10.1084/jem.20161674.

7. M. F. Gulen, U. Koch, S. M. Haag, F. Schuler, L. Apetoh, A. Villunger, F. Radtke, A. Ablasser, Signalling strength determines proapoptotic functions of STING. *Nat Commun* **8**, 427 (2017).

8. A. Goto, K. Okado, N. Martins, H. Cai, V. Barbier, O. Lamiable, L. Troxler, E. Santiago, L. Kuhn, D. Paik, N. Silverman, A. Holleufer, R. Hartmann, J. Liu, T. Peng, J. A. Hoffmann, C.

Meignin, L. Daeffler, J.-L. Imler, The Kinase IKKβ Regulates a STING-and NF-κB-Dependent Antiviral Response Pathway in Drosophila. *Immunity* **52**, 200 (2020).

9. B. R. Morehouse, A. A. Govande, A. Millman, A. F. A. Keszei, B. Lowey, G. Ofir, S. Shao, R. Sorek, P. J. Kranzusch, STING cyclic dinucleotide sensing originated in bacteria. *Nature* **586**, 429–433 (2020).

10. A. Bridgeman, J. Maelfait, T. Davenne, T. Partridge, Y. Peng, A. Mayer, T. Dong, V. Kaever, P. Borrow, J. Rehwinkel, Viruses transfer the antiviral second messenger cGAMP between cells. *Science* **349**, 1228–32 (2015).

11. M. Gentili, J. Kowal, M. Tkach, T. Satoh, X. Lahaye, C. Conrad, M. Boyron, B. Lombard, S. Durand, G. Kroemer, D. Loew, M. Dalod, C. Thery, N. Manel, Transmission of innate immune signaling by packaging of cGAMP in viral particles. *Science* **349**, 1232–6 (2015).

12. L. Chauveau, A. Bridgeman, T. K. Tan, R. Beveridge, J. N. Frost, P. Rijal, I. Pedroza-Pacheco, T. Partridge, J. Gilbert-Jaramillo, M. L. Knight, X. Liu, R. A. Russell, P. Borrow, H. Drakesmith, A. R. Townsend, J. Rehwinkel, Inclusion of cGAMP within virus-like particle vaccines enhances their immunogenicity. *EMBO Rep.* **22** (2021), doi:10.15252/embr.202152447.

13. A. Perez-Diez, N. T. Joncker, K. Choi, W. F. N. Chan, C. C. Anderson, O. Lantz, P. Matzinger, CD4 cells can be more efficient at tumor rejection than CD8 cells. *Blood* **109**, 5346–5354 (2007).

14. O. De Henau, M. Rausch, D. Winkler, L. F. Campesato, C. Liu, D. H. Cymerman, S. Budhu, A. Ghosh, M. Pink, J. Tchaicha, M. Douglas, T. Tibbitts, S. Sharma, J. Proctor, N. Kosmider, K. White, H. Stern, J. Soglia, J. Adams, V. J. Palombella, K. McGovern, J. L. Kutok, J. D. Wolchok, T. Merghoub, Overcoming resistance to checkpoint blockade therapy by targeting PI3Kγ in myeloid cells. *Nature* **539**, 443–447 (2016).

15. A. Hotblack, A. Holler, A. Piapi, S. Ward, H. J. Stauss, C. L. Bennett, Tumor-Resident Dendritic Cells and Macrophages Modulate the Accumulation of TCR-Engineered T Cells in Melanoma. *Mol. Ther.* **26**, 1471–1481 (2018).

16. R. Mattiuz, C. Brousse, M. Ambrosini, J. Cancel, G. Bessou, J. Mussard, A. Sanlaville, C. Caux, N. Bendriss-Vermare, J. Valladeau-Guilemond, M. Dalod, K. Crozat, Type 1 conventional dendritic cells and interferons are required for spontaneous $CD4^+$ and $CD8^+$ T-cell protective responses to breast cancer. *Clin. Transl. Immunol.* **10** (2021), doi:10.1002/cti2.1305.

17. M. K. Ruhland, E. W. Roberts, E. Cai, A. M. Mujal, K. Marchuk, C. Beppler, D. Nam, N. K. Serwas, M. Binnewies, M. F. Krummel, Visualizing Synaptic Transfer of Tumor Antigens among Dendritic Cells. *Cancer Cell* **37**, 786-799.e5 (2020).

18. F. Arce Vargas, A. J. S. Furness, I. Solomon, K. Joshi, L. Mekkaoui, M. H. Lesko, E. Miranda Rota, R. Dahan, A. Georgiou, A. Sledzinska, A. Ben Aissa, D. Franz, M. Werner Sunderland, Y. N. S. Wong, J. Y. Henry, T. O'Brien, D. Nicol, B. Challacombe, S. A. Beers, S. Turajlic, M. Gore, J. Larkin, C. Swanton, K. A. Chester, M. Pule, J. V. Ravetch, T. Marafioti, K. S. Peggs, S. A. Quezada, L. Spain, A. Wotherspoon, N. Francis, M. Smith, D. Strauss, A. Hayes,

A. Soultati, M. Stares, L. Spain, J. Lynch, N. Fotiadis, A. Fernando, S. Hazell, A. Chandra, L. Pickering, S. Rudman, S. Chowdhury, C. Swanton, M. Jamal-Hanjani, S. Veeriah, S. Shafi, J. Czyzewska-Khan, D. Johnson, J. Laycock, L. Bosshard-Carter, G. Goh, R. Rosenthal, P. Gorman, N. Murugaesu, R. E. Hynds, G. Wilson, N. J. Birkbak, T. B. K. Watkins, N. McGranahan, S. Horswell, R. Mitter, M. Escudero, A. Stewart, P. Van Loo, A. Rowan, H. Xu, S. Turajlic, C. Hiley, C. Abbosh, J. Goldman, R. K. Stone, T. Denner, N. Matthews, G. Elgar, S. Ward, J. Biggs, M. Costa, S. Begum, B. Phillimore, T. Chambers, E. Nye, S. Graca, M. Al Bakir, J. A. Hartley, H. L. Lowe, J. Herrero, D. Lawrence, M. Hayward, N. Panagiotopoulos, S. Kolvekar, M. Falzon, E. Borg, C. Simeon, G. Hector, A. Smith, M. Aranda, M. Novelli, D. Oukrif, S. M. Janes, R. Thakrar, M. Forster, T. Ahmad, S. M. Lee, D. Papadatos-Pastos, D. Carnell, R. Mendes, J. George, N. Navani, A. Ahmed, M. Taylor, J. Choudhary, Y. Summers, R. Califano, P. Taylor, R. Shah, P. Krysiak, K. Rammohan, E. Fontaine, R. Booton, M. Evison, P. Crosbie, S. Moss, F. Idries, L. Joseph, P. Bishop, A. Chaturved, A. M. Quinn, H. Doran, A. Leek, P. Harrison, K. Moore, R. Waddington, J. Novasio, F. Blackhall, J. Rogan, E. Smith, C. Dive, J. Tugwood, G. Brady, D. G. Rothwell, F. Chemi, J. Pierce, S. Gulati, B. Naidu, G. Langman, S. Trotter, M. Bellamy, H. Bancroft, A. Kerr, S. Kadiri, J. Webb, G. Middleton, M. Djearaman, D. Fennell, J. A. Shaw, J. Le Quesne, D. Moore, A. Nakas, S. Rathinam, W. Monteiro, H. Marshall, L. Nelson, J. Bennett, J. Riley, L. Primrose, L. Martinson, G. Anand, S. Khan, A. Amadi, M. Nicolson, K. Kerr, S. Palmer, H. Remmen, J. Miller, K. Buchan, M. Chetty, L. Gomersall, J. Lester, A. Edwards, F. Morgan, H. Adams, H. Davies, M. Kornaszewska, R. Attanoos, S. Lock, A. Verjee, M. MacKenzie, M. Wilcox, H. Bell, N. Iles, A. Hackshaw, Y. Ngai, S. Smith, N. Gower, C. Ottensmeier, S. Chee, B. Johnson, A. Alzetani, E. Shaw, E. Lim, P. De Sousa, M. T. Barbosa, A. Bowman, S. Jorda, A. Rice, H. Raubenheimer, C. Proli, M. E. Cufari, J. C. Ronquillo, A. Kwayie, H. Bhayani, M. Hamilton, Y. Bakar, N. Mensah, L. Ambrose, A. Devaraj, S. Buderi, J. Finch, L. Azcarate, H. Chavan, S. Green, H. Mashinga, A. G. Nicholson, K. Lau, M. Sheaff, P. Schmid, J. Conibear, V. Ezhil, B. Ismail, M. Irvin-sellers, V. Prakash, P. Russell, T. Light, T. Horey, S. Danson, J. Bury, J. Edwards, J. Hill, S. Matthews, Y. Kitsanta, K. Suvarna, P. Fisher, A. D. Keerio, M. Shackcloth, J. Gosney, P. Postmus, S. Feeney, J. Asante-Siaw, Fc-Optimized Anti-CD25 Depletes Tumor-Infiltrating Regulatory T Cells and Synergizes with PD-1 Blockade to Eradicate Established Tumors. *Immunity* **46**, 577–586 (2017).

19. M. J. Selby, J. J. Engelhardt, M. Quigley, K. A. Henning, T. Chen, M. Srinivasan, A. J. Korman, Anti-CTLA-4 Antibodies of IgG2a Isotype Enhance Antitumor Activity through Reduction of Intratumoral Regulatory T Cells. *Cancer Immunol. Res.* **1**, 32–42 (2013).

20. D. Sekar, L. Govene, M.-L. del Río, E. Sirait-Fischer, A. Fink, B. Brüne, J. Rodriguez-Barbosa, A. Weigert, Downregulation of BTLA on NKT Cells Promotes Tumor Immune Control in a Mouse Model of Mammary Carcinoma. *Int. J. Mol. Sci.* **19**, 752 (2018).

21. L. Deng, H. Liang, M. Xu, X. Yang, B. Burnette, A. Arina, X.-D. Li, H. Mauceri, M. Beckett, T. Darga, X. Huang, T. F. Gajewski, Z. J. Chen, Y.-X. Fu, R. R. Weichselbaum, STING-Dependent Cytosolic DNA Sensing Promotes Radiation-Induced Type I Interferon-Dependent Antitumor Immunity in Immunogenic Tumors. *Immunity* **41**, 843–852 (2014).

22. L. Andzinski, J. Spanier, N. Kasnitz, A. Kröger, L. Jin, M. M. Brinkmann, U. Kalinke, S. Weiss, J. Jablonska, S. Lienenklaus, Growing tumors induce a local STING dependent Type I IFN response in dendritic cells: STING Dependent Type I IFN Response in Dendritic Cells. *Int.*

J. Cancer **139**, 1350–1357 (2016).

23. Y. Wu, C.-H. A. Tang, C. Mealer, D. Bastian, M. Hanief Sofi, L. Tian, S. Schutt, H.-J. Choi, T. Ticer, M. Zhang, X. Sui, L. Huang, A. L. Mellor, C.-C. A. Hu, X.-Z. Yu, STING negatively regulates allogeneic T-cell responses by constraining antigen-presenting cell function. *Cell. Mol. Immunol.* **18**, 632–643 (2021).

24. O. Demaria, A. De Gassart, S. Coso, N. Gestermann, J. Di Domizio, L. Flatz, O. Gaide, O. Michielin, P. Hwu, T. V. Petrova, F. Martinon, R. L. Modlin, D. E. Speiser, M. Gilliet, STING activation of tumor endothelial cells initiates spontaneous and therapeutic antitumor immunity. *Proc. Natl. Acad. Sci.* **112**, 15408–15413 (2015).

25. B. J. Francica, A. Ghasemzadeh, A. L. Desbien, D. Theodros, K. E. Sivick, G. L. Reiner, L. Hix Glickman, A. E. Marciscano, A. B. Sharabi, M. L. Leong, S. M. McWhirter, T. W. Dubensky, D. M. Pardoll, C. G. Drake, TNFα and Radioresistant Stromal Cells Are Essential for Therapeutic Efficacy of Cyclic Dinucleotide STING Agonists in Nonimmunogenic Tumors. *Cancer Immunol. Res.* **6**, 422–433 (2018).

26. S. Jeong, M. J. Yang, S. Choi, J. Kim, G. Y. Koh, Refractoriness of STING therapy is relieved by AKT inhibitor through effective vascular disruption in tumour. *Nat. Commun.* **12**, 4405 (2021).

27. X. Lu, L. Miao, W. Gao, Z. Chen, K. J. McHugh, Y. Sun, Z. Tochka, S. Tomasic, K. Sadtler, A. Hyacinthe, Y. Huang, T. Graf, Q. Hu, M. Sarmadi, R. Langer, D. G. Anderson, A. Jaklenec, Engineered PLGA microparticles for long-term, pulsatile release of STING agonist for cancer immunotherapy. *Sci. Transl. Med.* **12**, eaaz6606 (2020).

28. D. R. Wilson, R. Sen, J. C. Sunshine, D. M. Pardoll, J. J. Green, Y. J. Kim, Biodegradable STING agonist nanoparticles for enhanced cancer immunotherapy. *Nanomedicine Nanotechnol. Biol. Med.* **14**, 237–246 (2018).

29. S. C. Jang, K. D. Economides, R. J. Moniz, C. L. Sia, N. Lewis, C. McCoy, T. Zi, K. Zhang, R. A. Harrison, J. Lim, J. Dey, M. Grenley, K. Kirwin, N. L. Ross, R. Bourdeau, A. Villiger-Oberbek, S. Estes, K. Xu, J. Sanchez-Salazar, K. Dooley, W. K. Dahlberg, D. E. Williams, S. Sathyanarayanan, ExoSTING, an extracellular vesicle loaded with STING agonists, promotes tumor immune surveillance. *Commun. Biol.* **4**, 497 (2021).

30. K. M. McAndrews, S. P. Y. Che, V. S. LeBleu, R. Kalluri, Effective delivery of STING agonist using exosomes suppresses tumor growth and enhances antitumor immunity. *J. Biol. Chem.* **296**, 100523 (2021).

31. X. Sewald, M. S. Ladinsky, P. D. Uchil, J. Beloor, R. Pi, C. Herrmann, N. Motamedi, T. T. Murooka, M. A. Brehm, D. L. Greiner, L. D. Shultz, T. R. Mempel, P. J. Bjorkman, P. Kumar, W. Mothes, Retroviruses use CD169-mediated trans-infection of permissive lymphocytes to establish infection. *Science* **350**, 563–7 (2015).

32. I. K. Vila, H. Chamma, A. Steer, M. Saccas, C. Taffoni, E. Turtoi, L. S. Reinert, S. Hussain, J. Marines, L. Jin, X. Bonnefont, M. Hubert, O. Schwartz, S. R. Paludan, G. Van Simaeys, G.

Doumont, B. Sobhian, D. Vlachakis, A. Turtoi, N. Laguette, STING orchestrates the crosstalk between polyunsaturated fatty acid metabolism and inflammatory responses. *Cell Metab.* **34**, 125-139.e8 (2022).

33. Y. Hou, H. Lu, J. Li, Z. Guan, J. Zhang, W. Zhang, C. Yin, L. Sun, Y. Zhang, H. Jiang, A photoaffinity labeling strategy identified EF1A1 as a binding protein of cyclic dinucleotide 2′3′-cGAMP. *Cell Chem. Biol.* **29**, 133-144.e20 (2022).

34. D. Acharya, R. Reis, M. Volcic, G. Liu, M. K. Wang, B. S. Chia, R. Nchioua, R. Groß, J. Münch, F. Kirchhoff, K. M. J. Sparrer, M. U. Gack, Actin cytoskeleton remodeling primes RIG-I-like receptor activation. *Cell* **185**, 3588-3602.e21 (2022).

35. T. Lança, J. Ungerbäck, C. Da Silva, T. Joeris, F. Ahmadi, J. Vandamme, M. Svensson-Frej, A. M. Mowat, K. Kotarsky, M. Sigvardsson, W. W. Agace, IRF8 deficiency induces the transcriptional, functional, and epigenetic reprogramming of cDC1 into the cDC2 lineage. *Immunity* **55**, 1431-1447.e11 (2022).

36. D. Zhivaki, F. Borriello, O. A. Chow, B. Doran, I. Fleming, D. J. Theisen, P. Pallis, A. K. Shalek, C. L. Sokol, I. Zanoni, J. C. Kagan, Inflammasomes within Hyperactive Murine Dendritic Cells Stimulate Long-Lived T Cell-Mediated Anti-tumor Immunity. *Cell Rep.* **33**, 108381 (2020).

37. P. Kozik, M. Gros, D. N. Itzhak, L. Joannas, S. Heurtebise-Chrétien, P. A. Krawczyk, P. Rodríguez-Silvestre, A. Alloatti, J. G. Magalhaes, E. Del Nery, G. H. H. Borner, S. Amigorena, Small Molecule Enhancers of Endosome-to-Cytosol Import Augment Anti-tumor Immunity. *Cell Rep.* **32**, 107905 (2020).

38. Z. Liao, L. M. Jaular, E. Soueidi, M. Jouve, D. C. Muth, T. H. Schøyen, T. Seale, N. J. Haughey, M. Ostrowski, C. Théry, K. W. Witwer, Acetylcholinesterase is not a generic marker of extracellular vesicles. *J. Extracell. Vesicles* **8**, 1628592 (2019).

39. M. R. Junttila, S. Saarinen, T. Schmidt, J. Kast, J. Westermarck, Single-step ***Strep*** -tag® purification for the isolation and identification of protein complexes from mammalian cells. *PROTEOMICS* **5**, 1199–1203 (2005).

40. P. Soriano, The PDGF alpha receptor is required for neural crest cell development and for normal patterning of the somites. *Dev. Camb. Engl.* **124**, 2691–2700 (1997).

41. S. J. Pettitt, Q. Liang, X. Y. Rairdan, J. L. Moran, H. M. Prosser, D. R. Beier, K. C. Lloyd, A. Bradley, W. C. Skarnes, Agouti C57BL/6N embryonic stem cells for mouse genetic resources. *Nat. Methods* **6**, 493–495 (2009).

42. C. I. Rodríguez, F. Buchholz, J. Galloway, R. Sequerra, J. Kasper, R. Ayala, A. F. Stewart, S. M. Dymecki, High-efficiency deleter mice show that FLPe is an alternative to Cre-loxP. *Nat. Genet.* **25**, 139–140 (2000).

43. A. Alloatti, F. Kotsias, E. Hoffmann, S. Amigorena, Evaluation of Cross-presentation in Bone Marrow-derived Dendritic Cells in vitro and Splenic Dendritic Cells ex vivo Using Antigen-

coated Beads. *BIO-Protoc.* **6** (2016), doi:10.21769/BioProtoc.2015.

Acknowledgements

We thank S. Amigorena, V. Soumelis, J. Rehwinkel, U. Kalinke and N. de Silva for discussions, A. Loverre, X. Lahaye and C. Conrad for help with experiments, CIPHE for their assistance in the breeding and shipment of mice, J. Helft for access to MMTV-PyMT mice.

Funding: This work was supported by Stimunity, Institut Curie (in particular the PIC TME and TMP to C.H.), Fondation Carnot, INSERM, Association Nationale de la Recherche et de la Technologie (Cifre to A.B.), European Research Council (ERC-2016-PoC STIMUNITY), Fondation BMS, Fondation pour la Recherche Médicale (EQU202103012774), Cancéropôle Ile-de-France (STINGTARGET), Agence Nationale de La Recherche (LABEX DCBIOL, ANR-10-IDEX-0001-02 PSL, ANR-11-LABX-0043), the MSDAVENIR Fund (to B.M.), INCa (PLBIO 2018-152 to M.D., INCA 2016-1-PL BIO-02-ICR-1), France 2030 investment plan Initiative d'Excellence d'Aix-Marseille Université (A*MIDEX AMX-19-IET-001) (PhD fellowship to R.A.), and the Investissement d'Avenir program PHENOMIN (French National Infrastructure for mouse Phenogenomics; ANR10-INBS-07 to B.M).

Author contributions: B.J. performed most experiments and analyzed data. A.B. performed a set of in vitro experiments. C.H., F.D., E.D., J.D., P.S., Y.G., R.A. and C.B. contributed to experiments. C.S., R.K., I.W., E.P., M.D., C.H., and H.S. suggested experiments and contributed to data analysis and interpretations. B.M. and F.F. conceived and developed the STING-OST^{fl} mice. S.C. developed Randmice. S.C. and N.M. conceived the study. N.M. and B.J. prepared figures and wrote the manuscript.

Competing interests: NM and SC are co-founders of the biotech Stimunity. SC is CEO of Stimunity. NM is scientific consultant of Stimunity. IW and RK are advisors of Stimunity. IW represents Portage BioTech at the board of Stimunity. Stimunity develops cGAMP-VLP in

cancer immunotherapy. CH is currently employed by the company Owkin. CH serves as advisor and has received honoraria from Nanobiotix.

Data and materials availability: Request for STING-OST^{fl} mice should be addressed to B. Malissen and should be covered by a material transfer agreement. All data needed to evaluate the conclusions of the paper are present in the paper or the Supplementary Materials.

Figure Legends

Figure 1 cGAMP-VLP induces tumor-specific T cell responses in a non-immunogenic tumor model

(A) Overview of the experimental design (TW = twice weekly). Treatments were initiated on palpable tumors (15-20 mm^3 range).

(B) Concentrations of IFN-α, IFN-β, IL-6 and TNF-α in the serum of B16-OVA tumor-bearing mice 3 hours after treatment (bar at mean + SEM, $N = 6$ to 24 mice per group, combined from 2 independent experiments, Kruskal-Wallis with Dunn post-test, LLOQ = lower limit of quantification, ULOQ = upper limit of quantification).

(C) Growth curves of individual B16-OVA tumors treated as indicated. Vertical dotted line indicates the death of the last mouse in the PBS-injected group. The number of completely responding mice followed by the number of total mice in each group is indicated.

(D) Mean growth over time of B16-OVA tumors treated as indicated (line at mean + SEM, $N = 6$ to 12 mice per group, combined from 2 independent experiments).

(E) Survival of B16-OVA tumor-bearing mice treated as indicated (log-rank Mantel-Cox test).

(F) OVA-specific CD8 (OVA-I) and CD4 (OVA-II) T cell responses in blood, assessed by IFN-γ ELISPOT (bar at mean + SEM, $N = 6$ to 12 mice per group, combined from 2 independent experiments, Kruskal-Wallis test with Dunn post-test).

* $p < 0.05$, ** $p < 0.01$, *** $p < 0.001$, **** $p < 0.0001$.

Figure 2 Tumor specific T-cell responses elicited by cGAMP-VLP translate into abscopal synergy with anti-PD1.

(A) Overview of the experimental design. Treatments were initiated on palpable tumors.

(B) Concentrations of IFN-α, IFN-β, IL-6 and TNF-α in the serum of B16-OVA dual tumor-bearing mice 3 hours after treatment (bar at mean + SEM, N = 6 to 24 mice per group, combined from 2 independent experiments, Kruskal-Wallis with Dunn post-test, LLOQ = lower limit of quantification, ULOQ = upper limit of quantification).

(C) OVA-specific CD8 (OVA-I) and CD4 (OVA-II) T cell responses in blood, assess by IFN-γ ELISPOT (bar at mean + SEM, N = 6 to 12 mice per group, combined from 2 independent experiments, Kruskal-Wallis with Dunn post-test).

(D) Growth curves of individual injected and distal B16-OVA tumors treated as indicated. Vertical dotted line indicates the death of the last mouse in the PBS-injected group.

(E) Mean growth over time of B16-OVA injected and distal tumors treated as indicated (line at mean + SEM, N = 6 to 12 mice per group, combined from 2 independent experiments).

(F) Distal tumor size at the indicated days in treated mice, for groups that did not reach ethical limits (line at mean + SEM, N = 12 mice per group, combined from 2 independent experiments, Kurskal-Wallis with Dunn post-test for day 27, Mann-Whitney for day 31).

(G) Survival of mice after secondary challenge. In complete responding mice, B16-OVA cells were injected 80 days from the first injection of tumor cells and treatments (combined from 3 experiments with single or dual tumors at the first injection, Gehan-Breslow-Wilcoxon test on cGAMP-VLP + anti-PD1 vs ADU-S100 + anti-PD1).

* $p < 0.05$, ** $p < 0.01$, *** $p < 0.001$, **** $p < 0.0001$.

Figure 3 The anti-tumor effect of cGAMP-VLP requires host STING and T lymphocytes.

(A) Overview of the experimental design using B16-OVA dual tumor-bearing mice (WT, *Sting1*$^{-/-}$ or *Rag2*$^{-/-}$). Treatments were initiated on palpable tumors.

(B) Concentrations of IFN-α, IL-6 and TNF-α in the serum 3 hours after the first treatment by i.t. injection of PBS, 50 µg ADU-S100 or 50 ng cGAMP-VLP (bar at mean + SEM, $N = 8$ to 16 mice per group, combined from 2 independent experiments, Kruskal-Wallis with Dunn post-test on the whole dataset, LLOQ = lower limit of quantification, ULOQ = upper limit of quantification).

(C) OVA-specific CD8 (OVA-I) and CD4 (OVA-II) T cell responses in blood of WT, *Sting1*$^{-/-}$ or *Rag2*$^{-/-}$ mice 17 days after tumor implantation, assessed by IFN-γ ELISPOT (bar at mean + SEM, $N = 11$ to 12 mice per group, combined from 2 independent experiments, Kruskal-Wallis with Dunn post-test). Mice were randomized at day 7 and treated by i.t. injection at days 7, 10 and 13.

(D) Size of injected and distal tumors 16 days after tumor implantation in WT, *Sting1*$^{-/-}$ or *Rag2*$^{-/-}$ treated mice (line at mean + SEM, $N = 16$ mice per group except $N = 15$ for WT PBS group, combined from 2 independent experiments, Kruskal-Wallis with Dunn post-test).

(E) Survival of B16-OVA dual tumor-bearing mice (WT, *Sting1*$^{-/-}$ or *Rag2*$^{-/-}$) treated as indicated (log-rank Mantel-Cox test). * $p < 0.05$, ** $p < 0.01$, *** $p < 0.001$, **** $p < 0.0001$.

Figure 4 Differential T cell subset composition in response to cGAMP-VLP over ADU-S100.

(A) Overview of the experiment.

(B) Frequency of immune cells (%CD45.2$^+$ within total live cells), NK cells (%NK1.1$^+$ within CD45.2$^+$), TCRβ$^+$CD4$^+$ T cells (within CD45.2$^+$), TCRβ$^+$CD8$^+$ T cells (within CD45.2$^+$), Tregs (%FoxP3$^+$CD25$^+$ within CD45.2$^+$TCRβ$^+$CD4$^+$) and B cells (%CD19$^+$ within CD45.2$^+$) in B16-OVA dual tumor-bearing mice treated as indicated at days 7, 10 and 13 and analyzed at day 14. Treatments were started on tumors of 10-20 mm3 average volume per group. Data combined from groups with and without anti-PD1 ($N = 6$ to 8 mice per group, Brown-Forsythe and Welch ANOVA test).

(C) Frequency of central memory (CM, gated as $CD44^+CD62L^+$ within $CD45.2^+TCR\beta^+CD8^+$ or $CD4^+$) and effector memory (EM, gated as $CD44^+CD62L^-$ within $CD45.2^+TCR\beta^+CD8^+$ or $CD4^+$) T cells in the indicated organs ($N = 8$ mice per group, Brown-Forsythe and Welch ANOVA test).

(D) Frequency of $CD69^+$ cells within $CD45.2^+TCR\beta^+CD8^+$ and $CD45.2^+TCR\beta^+CD4^+$ T cells in the indicated organs ($N = 6$ to 8 mice per group, Brown-Forsythe and Welch ANOVA test).

* $p < 0.05$, ** $p < 0.01$, *** $p < 0.001$, **** $p < 0.0001$.

Figure 5 Anti-tumor effect of cGAMP-VLP requires STING in dendritic cells

(A) Outline of the experiment using B16-OVA dual tumor-bearing mice (STING-OST^{fl}, STING-$OST^{\Delta LysM}$ or STING-$OST^{\Delta Cd11c}$). Treatments were initiated on palpable tumors

(B) Concentrations of IFN-α and IL-6 in the serum of STING-OST^{fl} or STING-$OST^{\Delta LysM}$ mice 3 hours after the first treatment by i.t. injection of PBS, 50 µg ADU-S100 or 50 ng cGAMP-VLP (bar at mean + SEM, $N = 14$ mice per group, combined from 2 independent experiments, Kruskal-Wallis with Dunn post-test, LLOQ = lower limit of quantification, ULOQ = upper limit of quantification).

(C) OVA-specific CD8 (OVA-I) and CD4 (OVA-II) T cell responses in blood of STING-OST^{fl} or STING-$OST^{\Delta LysM}$ mice treated as indicated, 16 days after tumor implantation, assessed by IFN-γ ELISPOT (bar at mean + SEM, $N = 12$ to 14 mice per group combined from 2 independent experiments, Kruskal-Wallis with Dunn post-test).

(D) Size over time of injected and distal B16-OVA tumors in STING-OST^{fl} or STING-$OST^{\Delta LysM}$ mice treated as indicated ($N = 14$ mice per group combined from 2 independent experiments, line at mean ± SEM, Sidak's multiple comparisons 2-way ANOVA test).

(E) Concentrations of IFN-α and IL-6 in the serum of STING-OST^{fl} or STING-$OST^{\Delta LysM}$ mice 3 hours after the first treatment by i.t. injection of PBS, 50 µg ADU-S100 or 50 ng cGAMP-VLP

(bar at mean + SEM, N = 12 to 14 mice per group, combined from 2 independent experiments, Kruskal-Wallis with Dunn post-test, LLOQ = lower limit of quantification, ULOQ = upper limit of quantification).

(F) OVA-specific CD8 (OVA-I) and CD4 (OVA-II) T cell responses in blood of STING-OST^{fl} or STING-OST$^{\Delta Cd11c}$ mice treated as indicated, 16 days after tumor implantation, assessed by IFN-γ ELISPOT (bar at mean + SEM, N = 11 to 14 mice per group combined from 2 independent experiments, Kruskal-Wallis with Dunn post-test).

(G) Size over time of injected and distal B16-OVA tumors in STING-OST^{fl} or STING-OST$^{\Delta Cd11c}$ mice treated as indicated (N = 12 to 14 mice per group combined from 2 independent experiments, line at mean ± SEM, Sidak's multiple comparisons 2-way ANOVA test).

* $p < 0.05$, ** $p < 0.01$, *** $p < 0.001$, **** $p < 0.0001$.

Figure 6 T-cell mediated anti-tumor activity of cGAMP-VLP requires cDC1

(A) Analysis of dendritic cells, outline of the experiment.

(B) cDC1 (XCR1$^+$CD172$^-$) and cDC2 (XCR1$^-$CD172a$^+$) in live CD45$^+$MHC-II$^+$CD11c$^+$ cells in tumors treated as indicated at day 7 and analyzed at day 8 (representative of N = 3 independent experiments).

(C) Frequency of cDC1 (%MHC-II$^+$CD11C$^+$XCR1$^+$ within CD45.2$^+$ live cells), cDC2 (%MHC-II$^+$CD11C$^+$CD172a$^+$ within CD45.2$^+$ live cells), CD80$^+$ and CD86$^+$ on cDC1 and cDC2 (based on isotype) in B16-OVA tumors treated as indicated. Data combined from 3 independent experiments (N = 4 to 8 mice per group, one-way ANOVA with Tukey test).

(D) Overview of the experimental design using B16-OVA tumor-bearing mice (WT or *Xcr1*^{DTA}). Treatments were initiated on palpable tumors. Some experiments included dual tumor-bearing mice.

(E) OVA-specific CD8 (OVA-I) and CD4 (OVA-II) T cell responses in blood of WT or *Xcr1*^{DTA} mice treated as indicated, 17 days after tumor implantation, assessed by IFN-γ ELISPOT (bar at mean + SEM, N = 8 to 12 mice per group combined from 3 independent experiments, Sidak's multiple comparisons 2-way ANOVA test).

(F) Size of injected tumors 17 days after tumor implantation in WT or *Xcr1*^{DTA} treated mice (line at mean + SEM, N = 8 to 12 mice per group combined from 3 independent experiments, 2-way ANOVA test with Tukey post-test).

* $p < 0.05$, ** $p < 0.01$, *** $p < 0.001$, **** $p < 0.0001$.

Figure 7 Sub-cutaneous injection of cGAMP-VLP induces anti-tumor synergy with tumor Treg depletion.

(A) Outline of the experiment using B16-OVA tumors to compare i.t. and s.c. injection routes of cGAMP-VLP. Treatments were started on tumors of 50 mm^3 average volume per group.

(B) Concentrations of IFN-α, IFN-β, IL-6 and TNF-α in the serum of mice 3 hours after the first treatment with PBS or 50 ng cGAMP-VLP injected by the i.t. or s.c. route (bar at mean + SEM, N = 9 to 11 mice per group, combined from 2 independent experiments, Kruskal-Wallis with Dunn post-test, LLOQ = lower limit of quantification, ULOQ = upper limit of quantification).

(C) Growth curves of individual B16-OVA tumors in mice treated as indicated (N = 18 mice per group combined from 3 independent experiments). Mice were randomized at day 7, and treated at days 7, 10 and 13 with cGAMP-VLP, and bi-weekly from day 7 for 3 weeks with anti-PD1.

(D) Size of tumor 17 days after tumor implantation in treated mice (line at mean + SEM, N = 18 mice per group combined from 3 independent experiments, Kruskal-Wallis with Dunn post-test).

(E) OVA-specific CD8 (OVA-I) and CD4 (OVA-II) T cell responses in blood of mice 16 days after tumor implantation, assessed by IFN-γ ELISPOT (bar at mean + SEM, $N = 12$ mice per group, combined from 2 independent experiments, Kruskal-Wallis with Dunn post-test).

(F) Survival of B16-OVA tumor-bearing mice treated as indicated (log-rank Mantel-Cox test, $N = 12$ mice per group combined from 2 independent experiments).

(G) Outline of the experiment using MCA-OVA tumors, cGAMP-VLP and a tumor Treg-depleting antibody (anti-CTLA4-m2a). Treatments were started on tumors of 50 mm^3 average volume per group.

(H) Fraction of $CD25^+FoxP3^+$ Tregs within $CD45.2^+TCR\beta^+CD4^+$ cells in spleen and tumor, 48 hours after last i.p. injection of αCTLA4-m2a or isotype ($N = 4$, 2 mice from 2 independent experiments were analyzed).

(I) CD8 T cell responses against p15 antigen in blood of mice 16 days after tumor implantation, assessed by IFN-γ ELISPOT (bar at mean + SEM, $N = 15$ mice per group, combined from 2 independent experiments, Kruskal-Wallis with Dunn post-test).

(J) Mean growth over time of MCA-OVA tumors treated as indicated (line at mean + SEM, $N = 15$ mice per group, combined from 2 independent experiments).

(K) Survival of MCA-OVA tumor-bearing mice treated as indicated ($N = 15$ mice per group, combined from 2 independent experiments, log-rank Mantel-Cox test).

* $p < 0.05$, ** $p < 0.01$, *** $p < 0.001$, **** $p < 0.0001$.

Figure 8 cGAMP-VLP is active against spontaneous tumors and in human tumor samples.

(A) Overview of the experimental design using MMTV-$PyMT^{+/-}$ spontaneous breast tumor-bearing mice. Treatments were started on tumors of 20-40 mm^3 average volume per group.

(B) Sum of the size of tumors at the first day of s.c. injection of cGAMP-VLP and anti-PD1, and 10 or 13 days later (line at mean + SEM, $N = 7$ mice per group combined from 3 independent cohorts, Mann Whitney test).

(C) Survival of MMTV-PyMT$^{+/-}$ tumor-bearing mice treated as indicated ($N = 7$ mice per group, combined from 3 independent cohorts, log-rank Mantel-Cox test).

(D) Outline of the experiment using human head & neck tumor and lymph node samples.

(E) Frequency of CD11c^{+}HLA-DR^{+} cells (within CD45^{+}Lin^{-} live cells) in head & neck tumors treated *in vitro* as indicated. Data combined from 2 independent experiments (two patients).

(F) Frequency of PDL1^{+} and CD83^{+} cells within cDC (live CD45^{+}Lin^{-}CD11c^{+}HLA-DR^{+}CD14^{-} CD1c^{+}) in lymph node samples treated as indicated. Data combined from 2 independent experiments (two patients).

** $p < 0.01$.

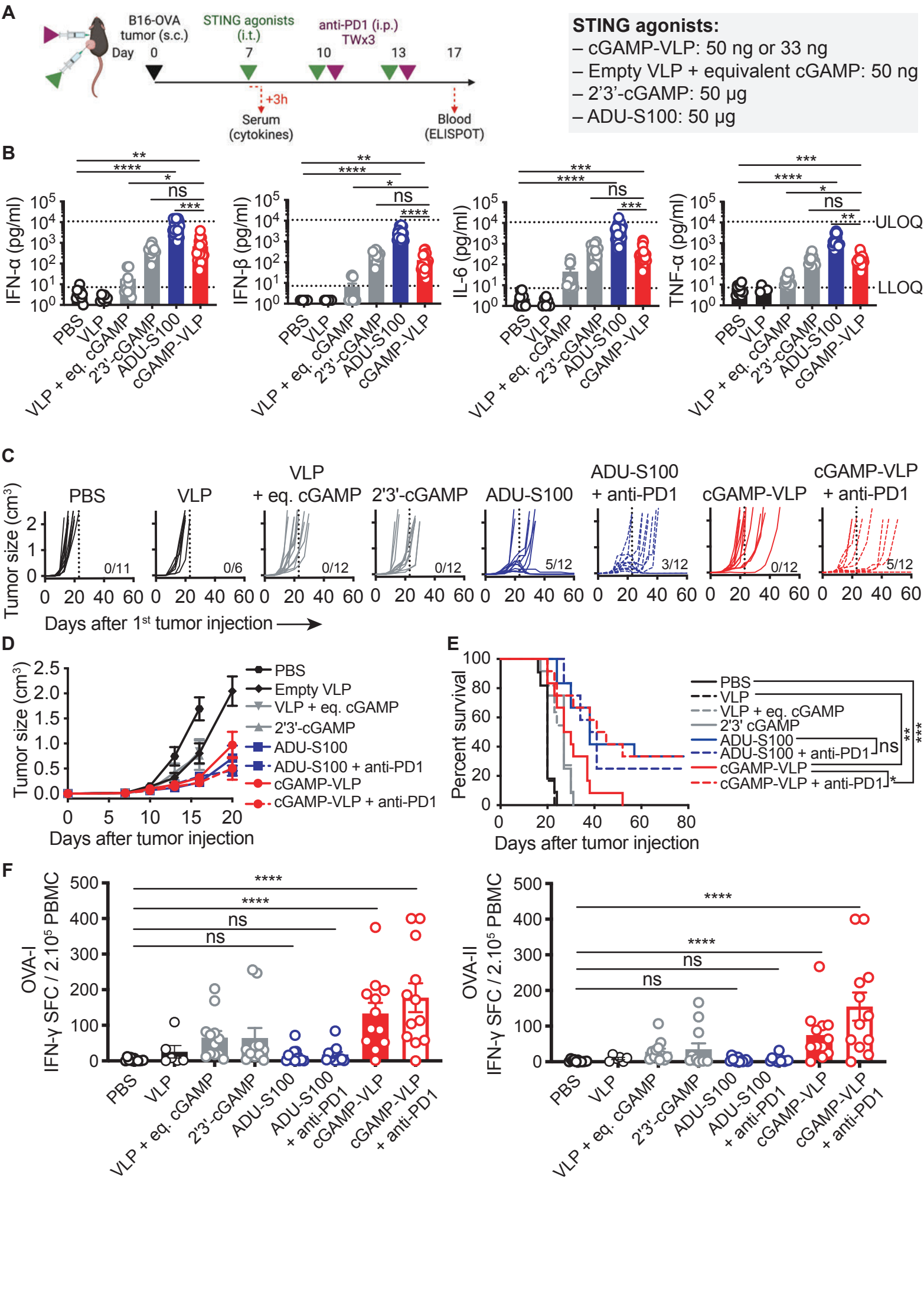
A
B16-OVA tumor (s.c.)
STING agonists (i.t.)
anti-PD1 (i.p.) TWx3
Day 0 7 10 13 17
+3h
Serum (cytokines)
Blood (ELISPOT)
STING agonists:
– cGAMP-VLP: 50 ng or 33 ng
– Empty VLP + equivalent cGAMP: 50 ng
– 2'3'-cGAMP: 50 µg
– ADU-S100: 50 µg
B
IFN-α (pg/ml)
IFN-β (pg/ml)
IL-6 (pg/ml)
TNF-α (pg/ml)
ULOQ
LLOQ
PBS
VLP
VLP + eq. cGAMP
2'3'-cGAMP
ADU-S100
cGAMP-VLP
C
PBS
VLP
VLP + eq. cGAMP
2'3'-cGAMP
ADU-S100
ADU-S100 + anti-PD1
cGAMP-VLP
cGAMP-VLP + anti-PD1
Tumor size (cm³)
0/11
0/6
0/12
0/12
5/12
3/12
0/12
5/12
Days after 1st tumor injection
D
Tumor size (cm³)
PBS
Empty VLP
VLP + eq. cGAMP
2'3'-cGAMP
ADU-S100
ADU-S100 + anti-PD1
cGAMP-VLP
cGAMP-VLP + anti-PD1
Days after tumor injection
E
Percent survival
PBS
VLP
VLP + eq. cGAMP
2'3' cGAMP
ADU-S100
ADU-S100 + anti-PD1
cGAMP-VLP
cGAMP-VLP + anti-PD1
Days after tumor injection
F
OVA-I
IFN-γ SFC / 2.10⁵ PBMC
OVA-II
IFN-γ SFC / 2.10⁵ PBMC
PBS
VLP
VLP + eq. cGAMP
2'3'-cGAMP
ADU-S100
ADU-S100 + anti-PD1
cGAMP-VLP
cGAMP-VLP + anti-PD1

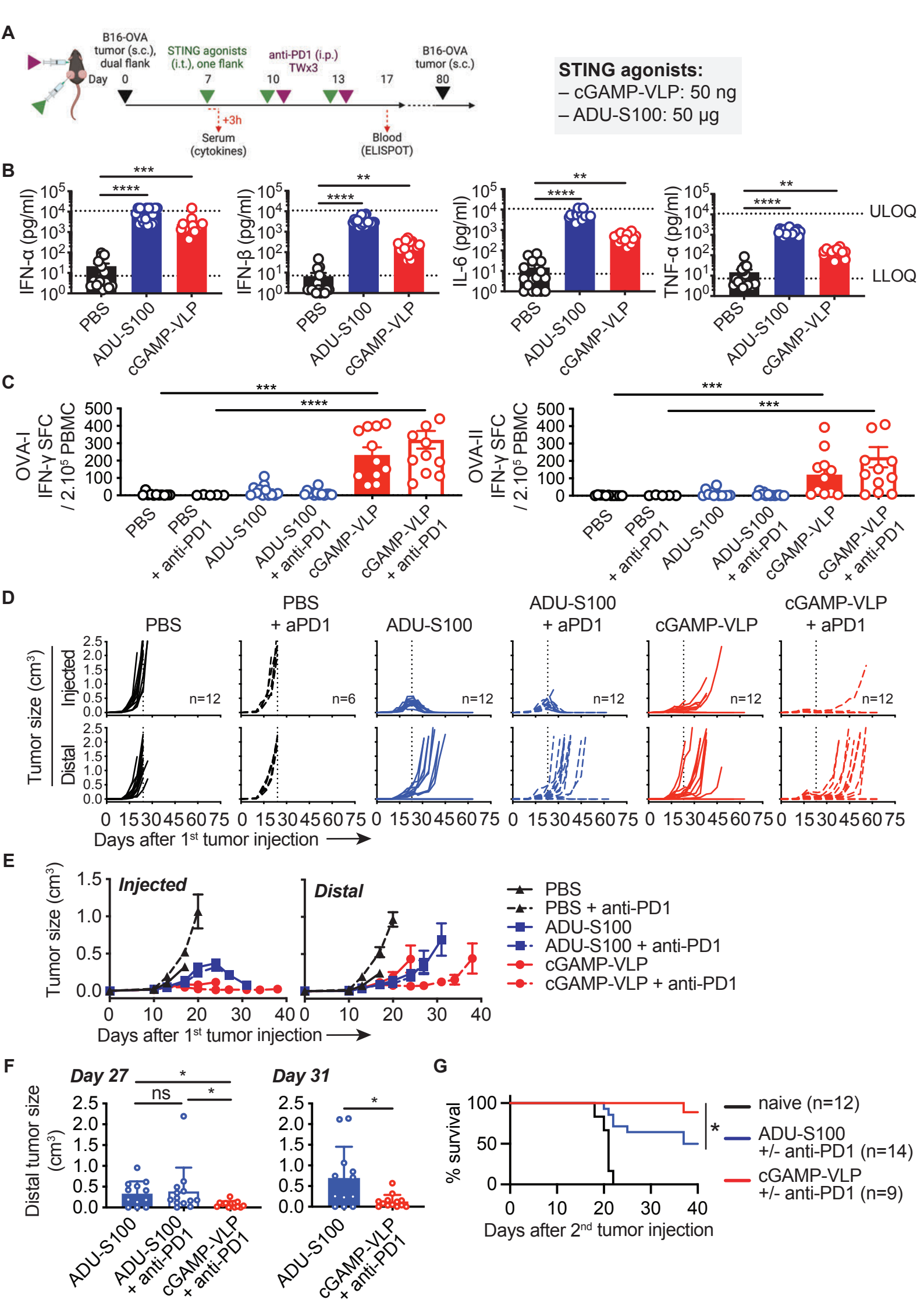
A
B16-OVA tumor (s.c.), dual flank
STING agonists (i.t.), one flank
anti-PD1 (i.p.) TWx3
B16-OVA tumor (s.c.)
Day 0 7 10 13 17 80
+3h
Serum (cytokines)
Blood (ELISPOT)
STING agonists:
– cGAMP-VLP: 50 ng
– ADU-S100: 50 µg
B
IFN-α (pg/ml)
IFN-β (pg/ml)
IL-6 (pg/ml)
TNF-α (pg/ml)
ULOQ
LLOQ
PBS
ADU-S100
cGAMP-VLP
C
OVA-I IFN-γ SFC / 2.10⁵ PBMC
OVA-II IFN-γ SFC / 2.10⁵ PBMC
PBS
PBS + anti-PD1
ADU-S100
ADU-S100 + anti-PD1
cGAMP-VLP
cGAMP-VLP + anti-PD1
D
Tumor size (cm³)
Injected
Distal
n=12
n=6
Days after 1st tumor injection
E
Injected
Distal
Tumor size (cm³)
Days after 1st tumor injection
PBS
PBS + anti-PD1
ADU-S100
ADU-S100 + anti-PD1
cGAMP-VLP
cGAMP-VLP + anti-PD1
F
Day 27
Day 31
Distal tumor size (cm³)
ns
G
% survival
Days after 2nd tumor injection
naive (n=12)
ADU-S100 +/- anti-PD1 (n=14)
cGAMP-VLP +/- anti-PD1 (n=9)

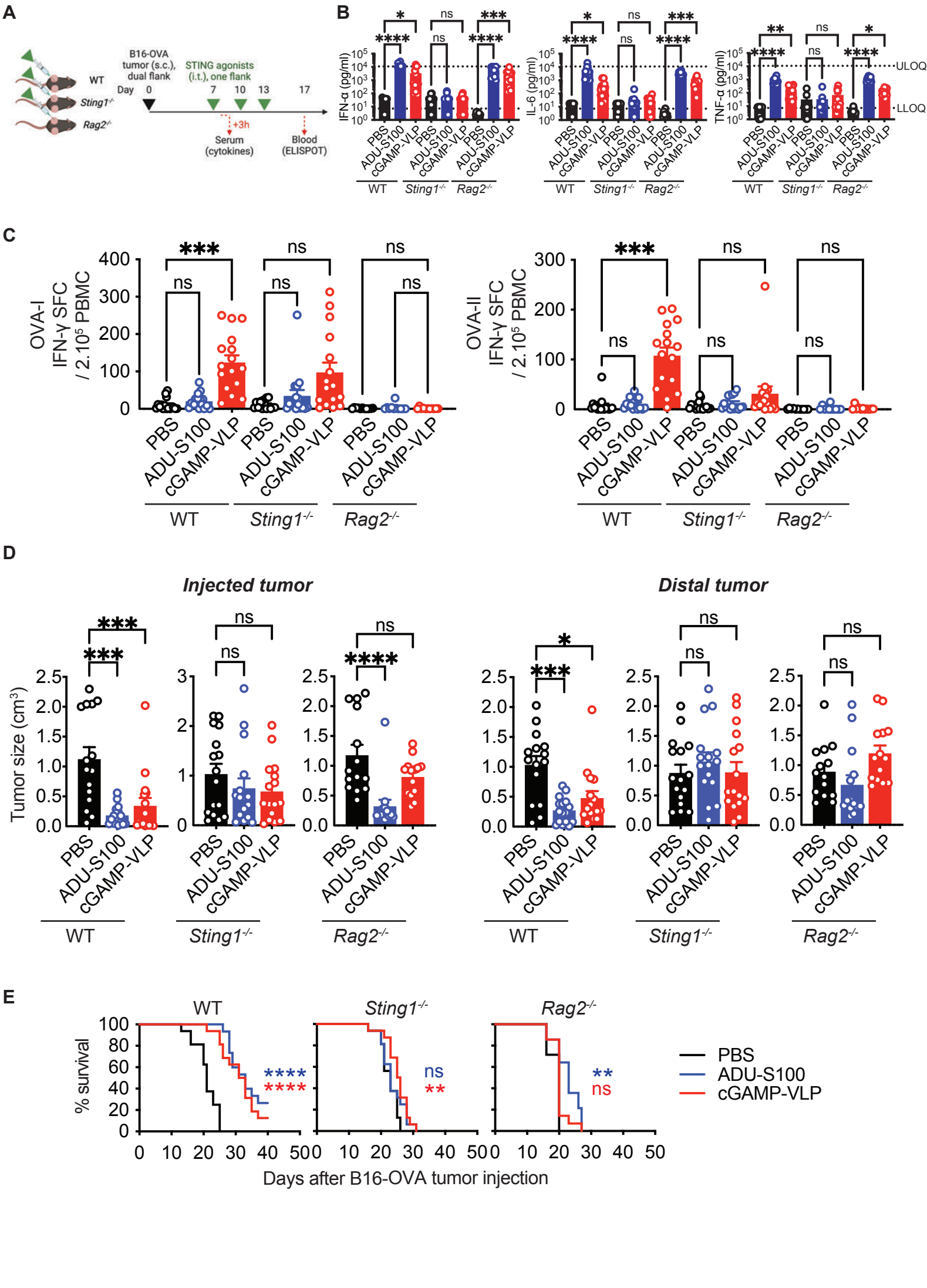
A
WT
Sting1-/-
Rag2-/-
B16-OVA tumor (s.c.), dual flank
STING agonists (i.t.), one flank
Day 0 7 10 13 17
+3h
Serum (cytokines)
Blood (ELISPOT)
B
IFN-α (pg/ml)
IL-6 (pg/ml)
TNF-α (pg/ml)
ULOQ
LLOQ
PBS
ADU-S100
cGAMP-VLP
WT
Sting1-/-
Rag2-/-
C
OVA-I IFN-γ SFC / 2.10^5 PBMC
OVA-II IFN-γ SFC / 2.10^5 PBMC
D
Injected tumor
Distal tumor
Tumor size (cm3)
E
% survival
Days after B16-OVA tumor injection
PBS
ADU-S100
cGAMP-VLP

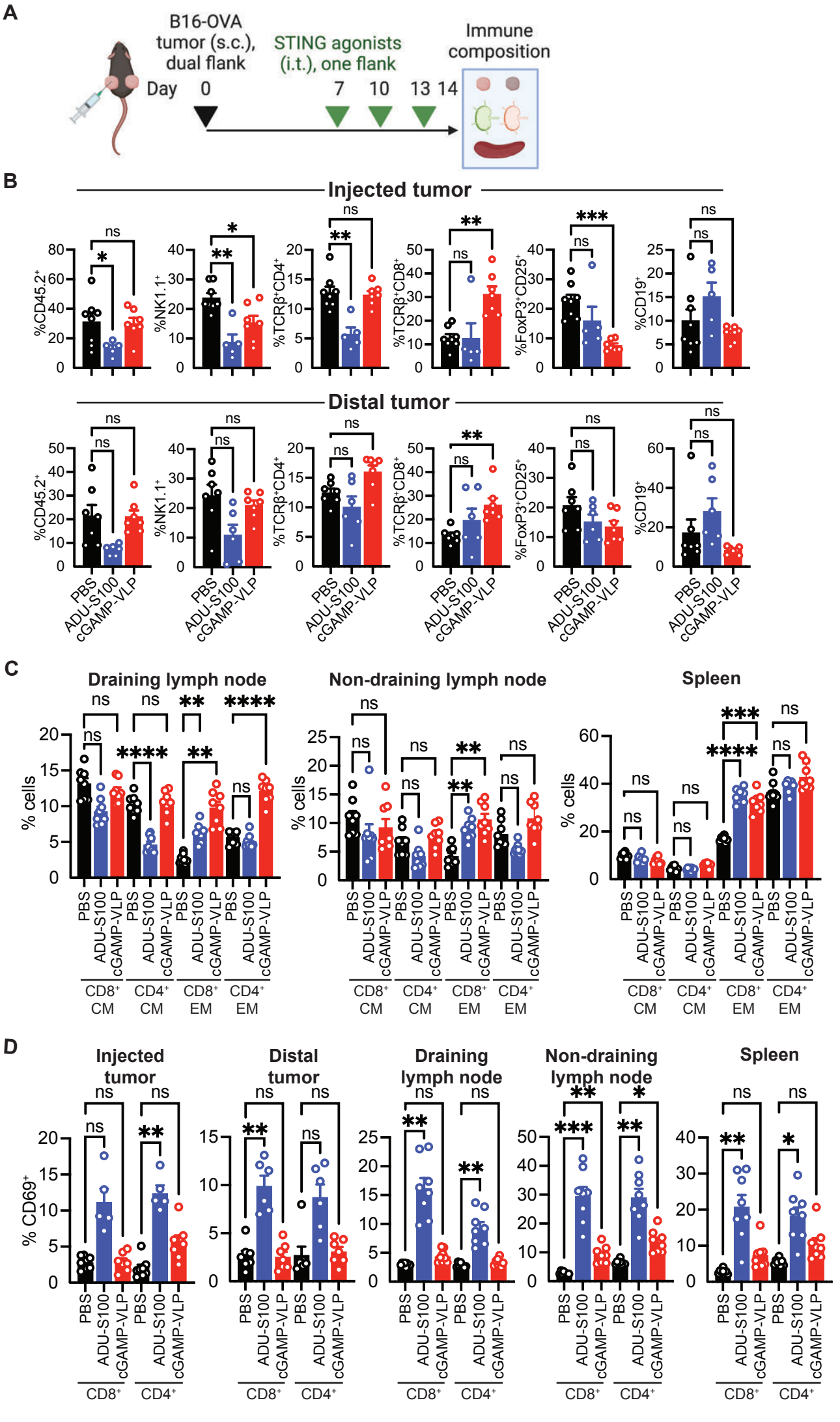
A
B16-OVA tumor (s.c.), dual flank
STING agonists (i.t.), one flank
Immune composition
Day 0 7 10 13 14
B
Injected tumor
Distal tumor
%CD45.2+
%NK1.1+
%TCRβ+CD4+
%TCRβ+CD8+
%FoxP3+CD25+
%CD19+
PBS
ADU-S100
cGAMP-VLP
C
Draining lymph node
Non-draining lymph node
Spleen
% cells
CD8+ CM
CD4+ CM
CD8+ EM
CD4+ EM
D
Injected tumor
Distal tumor
Draining lymph node
Non-draining lymph node
Spleen
% CD69+
CD8+
CD4+

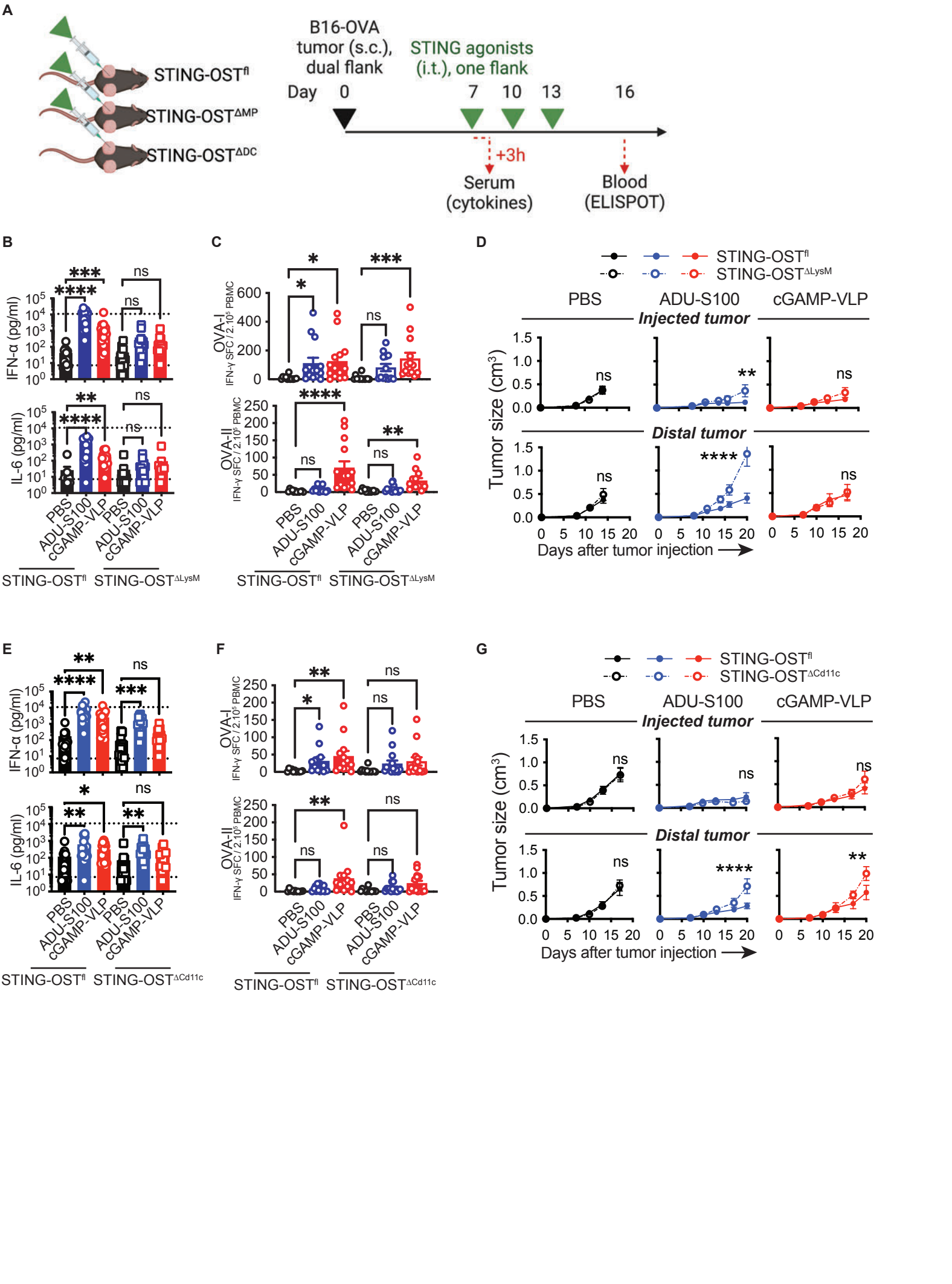
A
STING-OST^fl
STING-OST^ΔMP
STING-OST^ΔDC
B16-OVA tumor (s.c.), dual flank
STING agonists (i.t.), one flank
Day 0 7 10 13 16
+3h
Serum (cytokines)
Blood (ELISPOT)
B
IFN-α (pg/ml)
IL-6 (pg/ml)
PBS
ADU-S100
cGAMP-VLP
STING-OST^fl
STING-OST^ΔLysM
C
OVA-I IFN-γ SFC / 2.10^5 PBMC
OVA-II IFN-γ SFC / 2.10^5 PBMC
D
STING-OST^fl
STING-OST^ΔLysM
Injected tumor
Distal tumor
Tumor size (cm^3)
Days after tumor injection
E
STING-OST^ΔCd11c
F
G
STING-OST^ΔCd11c

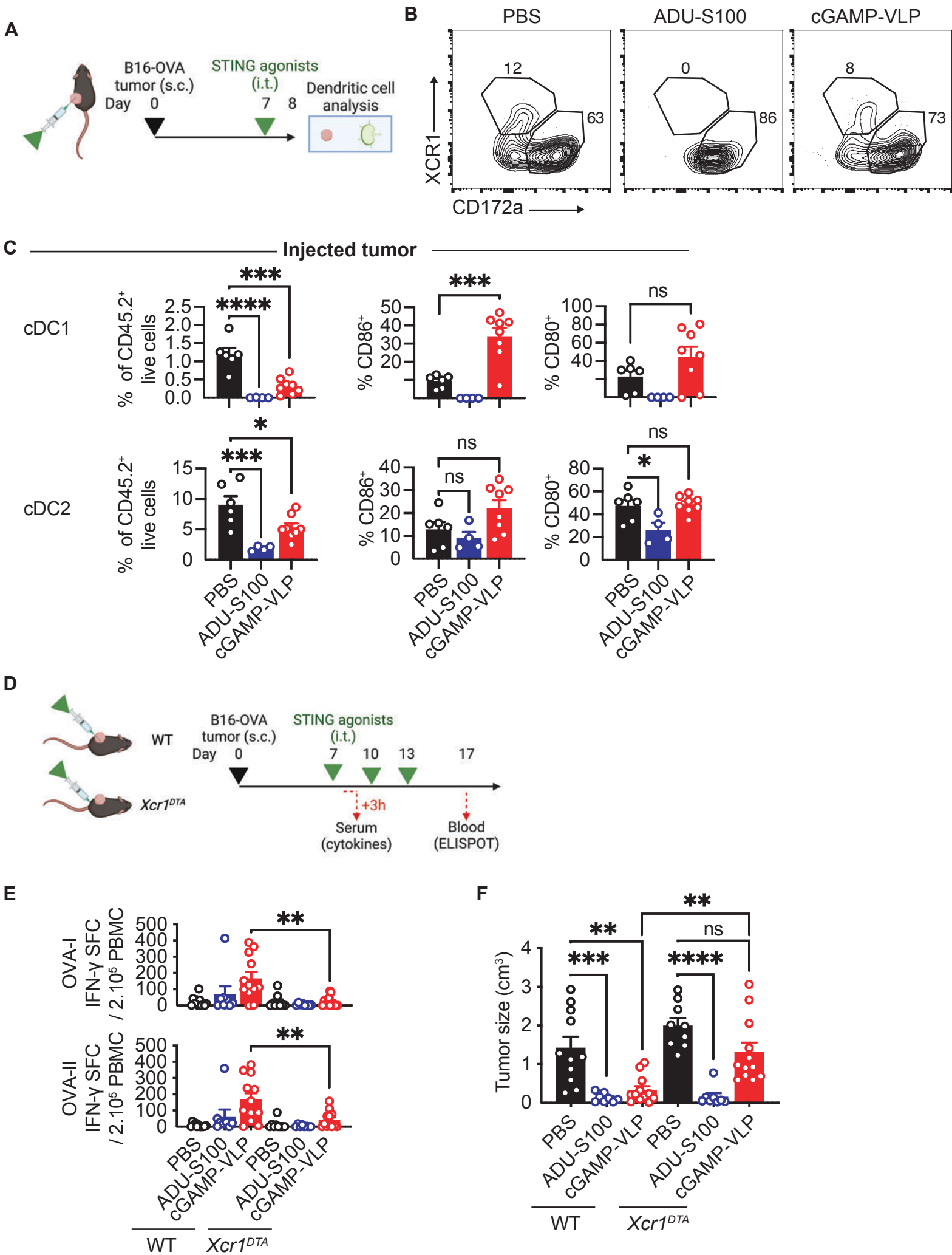
A
B16-OVA tumor (s.c.)
Day 0
STING agonists (i.t.)
7 8
Dendritic cell analysis
B
PBS
ADU-S100
cGAMP-VLP
12
63
0
86
8
73
XCR1
CD172a
C
Injected tumor
cDC1
cDC2
% of CD45.2+ live cells
% CD86+
% CD80+
PBS
ADU-S100
cGAMP-VLP
ns
D
WT
Xcr1DTA
B16-OVA tumor (s.c.)
Day 0
STING agonists (i.t.)
7 10 13 17
+3h
Serum (cytokines)
Blood (ELISPOT)
E
OVA-I IFN-γ SFC / 2.10⁵ PBMC
OVA-II IFN-γ SFC / 2.10⁵ PBMC
PBS
ADU-S100
cGAMP-VLP
WT
Xcr1DTA
F
Tumor size (cm³)
PBS
ADU-S100
cGAMP-VLP
WT
Xcr1DTA
ns

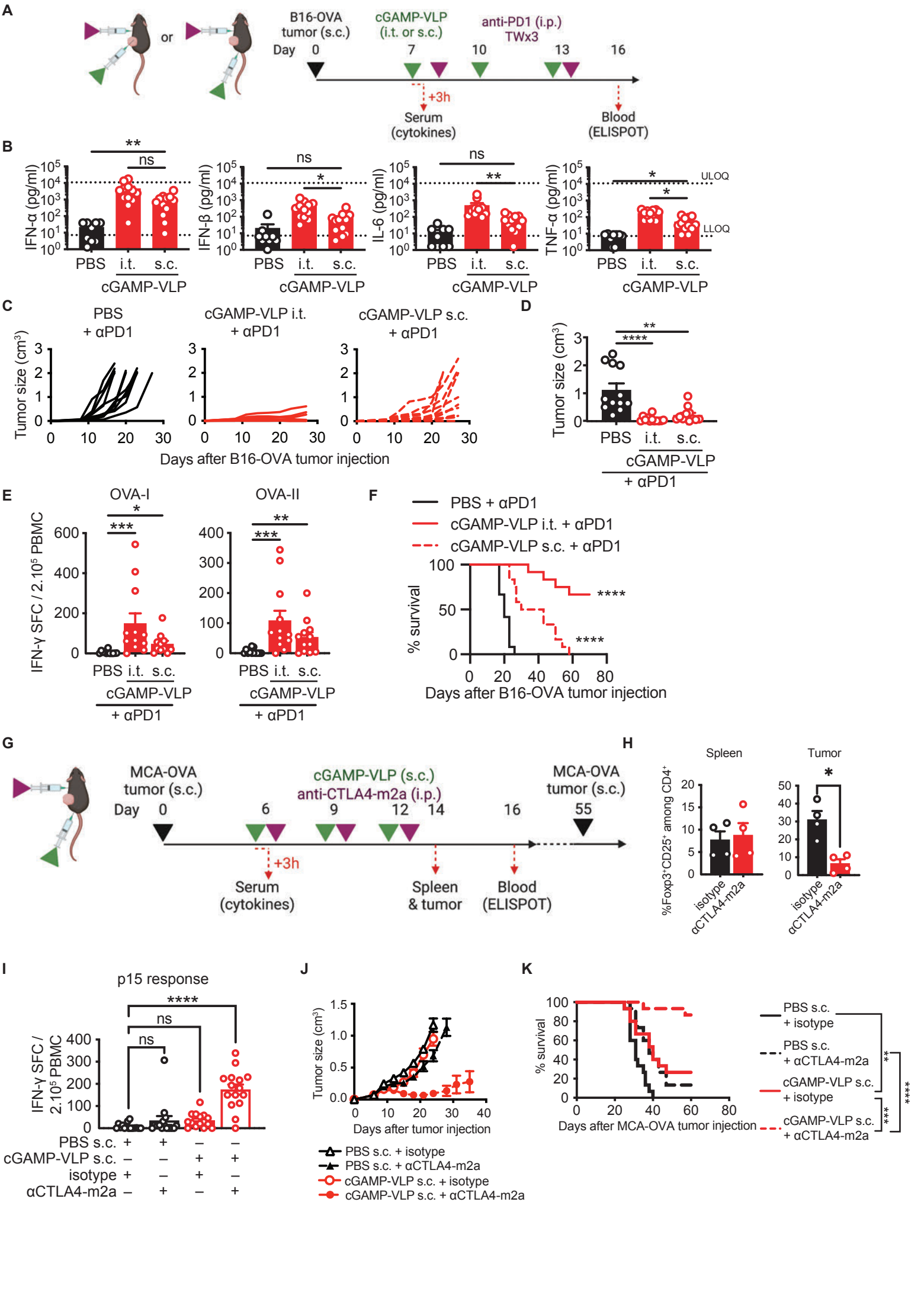
A
or
B16-OVA tumor (s.c.)
cGAMP-VLP (i.t. or s.c.)
anti-PD1 (i.p.) TWx3
Day 0 7 10 13 16
+3h
Serum (cytokines)
Blood (ELISPOT)
B
IFN-α (pg/ml)
IFN-β (pg/ml)
IL-6 (pg/ml)
TNF-α (pg/ml)
ULOQ
LLOQ
PBS i.t. s.c.
cGAMP-VLP
C
PBS + αPD1
cGAMP-VLP i.t. + αPD1
cGAMP-VLP s.c. + αPD1
Tumor size (cm³)
Days after B16-OVA tumor injection
D
Tumor size (cm³)
PBS i.t. s.c.
cGAMP-VLP + αPD1
E
OVA-I
OVA-II
IFN-γ SFC / 2.10⁵ PBMC
F
PBS + αPD1
cGAMP-VLP i.t. + αPD1
cGAMP-VLP s.c. + αPD1
% survival
Days after B16-OVA tumor injection
G
MCA-OVA tumor (s.c.)
cGAMP-VLP (s.c.)
anti-CTLA4-m2a (i.p.)
Day 0 6 9 12 14 16 55
+3h
Serum (cytokines)
Spleen & tumor
Blood (ELISPOT)
H
Spleen
Tumor
%Foxp3⁺CD25⁺ among CD4⁺
isotype
αCTLA4-m2a
I
p15 response
IFN-γ SFC / 2.10⁵ PBMC
PBS s.c. + + – –
cGAMP-VLP s.c. – – + +
isotype + – + –
αCTLA4-m2a – + – +
J
Tumor size (cm³)
Days after tumor injection
PBS s.c. + isotype
PBS s.c. + αCTLA4-m2a
cGAMP-VLP s.c. + isotype
cGAMP-VLP s.c. + αCTLA4-m2a
K
% survival
Days after MCA-OVA tumor injection
PBS s.c. + isotype
PBS s.c. + αCTLA4-m2a
cGAMP-VLP s.c. + isotype
cGAMP-VLP s.c. + αCTLA4-m2a

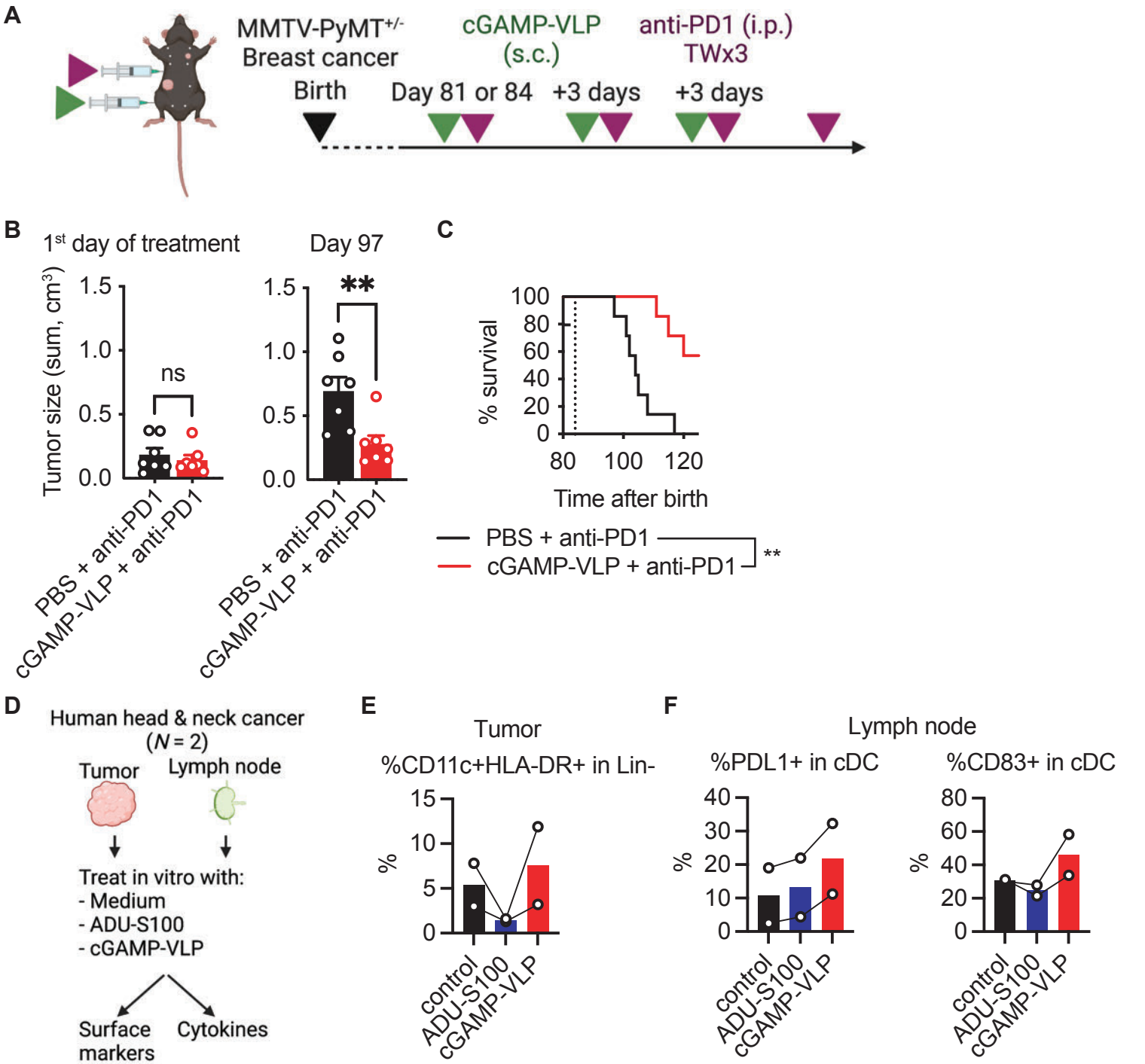
A
MMTV-PyMT+/-
Breast cancer
cGAMP-VLP
(s.c.)
anti-PD1 (i.p.)
TWx3
Birth
Day 81 or 84
+3 days
+3 days
B
1st day of treatment
Day 97
Tumor size (sum, cm3)
ns
**
PBS + anti-PD1
cGAMP-VLP + anti-PD1
C
% survival
Time after birth
PBS + anti-PD1
cGAMP-VLP + anti-PD1
**
D
Human head & neck cancer
(N = 2)
Tumor
Lymph node
Treat in vitro with:
- Medium
- ADU-S100
- cGAMP-VLP
Surface markers
Cytokines
E
Tumor
%CD11c+HLA-DR+ in Lin-
%
control
ADU-S100
cGAMP-VLP
F
Lymph node
%PDL1+ in cDC
%CD83+ in cDC

Supplementary Methods

Generation of STING-OST^{fl} knock-in mice

The mouse *Sting1* gene (also called Tmem173; ENSMUSG00000024349) was edited using a double-stranded HDR template (targeting vector) containing 867 and 1260 bp-long 5' and 3' homology arms, respectively. It included a loxP site and a frt-neo^{r}-frt cassette that were both inserted in intron 2, 110 bp upstream of the start codon, a Twin-Strep-tag-coding sequence (OST; *(39)*) that was appended at the 5' end of the first coding exon (exon 3), and a loxP site located in intron 3, 40 bp downstream of the 3' end of exon 3. The final targeting vector was abutted to a cassette coding for the diphtheria toxin fragment A *(40)*. Two sgRNA-containing pX330 plasmids (pSpCas9; Addgene, plasmid ID 42230) were constructed. In the first plasmid, two sgRNA-specifying oligonucleotide sequences (5'-CACCGAGTAGCCCATGGGACTAGC-3' and 5'-AAACGCTAGTCCCATGGGCTACTC-3') were annealed, generating overhangs for ligation into the BbsI site of plasmid pX330. In the second plasmid, two sgRNA-specifying oligonucleotide sequences (5'-CACCGTCAAGGGTGTGATACTTGC-3' and 5'-AAAC-GCAAGTATCACACCCTTGAC-3') were annealed and cloned into the BbsI site of plasmid pX330. The protospacer-adjacent motifs (PAM) corresponding to each sgRNA and present in the targeting vector were destroyed via silent mutations to prevent CRISPR-Cas9 cleavage. JM8.F6 C57BL/6N ES cells *(41)* were electroporated with 20 µg of targeting vector and 2.5 µg of each sgRNA-containing pX330 plasmid. After selection in G418, ES cell clones were screened for proper homologous recombination by Southern blot and PCR analysis. A neomycin specific probe was used to ensure that adventitious non-homologous recombination events had not occurred in the selected ES clones. Mutant ES cells were injected into BalbC/N blastocysts. Following germline transmission, excision of the frt-neo^{r}-frt cassette was achieved through genetic cross with transgenic mice expressing a FLP recombinase under the control of the actin promoter *(42)*. Two pairs of primers were used to distinguish the WT and edited *Tmem173* alleles. A pair of primers (sense 5'-TGTAGGATGCTATGTGCCCA-3' and antisense 5'-GATCCCAGCCCAACTCAGCT-3') amplified a 501 bp-long band in the case of the wild-type *Tmem173* allele and a 722 bp-long band in the case of the mutant allele.

The resulting STING-OST^{fl} mice (official name B6-*Tmem173*^{Tm1Ciphe} mice**)** have been established on a C57BL/6N background. They express a multitask *Tmem173* allele in which the third exon of the *Tmem173* allele is bracketed by *loxP* sequences and a sequence corresponding to an affinity Twin-Strep-Tag (OST) is appended at the 5' end of the ORF of the *Tmem173* gene. When bred to mice that express tissue-specific Cre recombinase, the resulting offspring will have exon 3 removed in the Cre-expressing tissues, resulting in cells lacking STING.

Western blotting

1 million cells were lysed in 100 µL of RIPA buffer (50 mM Tris HCl, 150 mM NaCl, 0.1% SDS, 0.5% DOC, 1% NP-40, 1X protease inhibitor cocktail (Roche; 1187358001)). Lysis was performed on ice for 30 minutes. Lysates were cleared by centrifugation at 19 000 *x g* for 20 minutes at 4°C, 4 µL of Laemmli 6x (12% SDS, 30% Glycerol, 0.375 M Tris-HCl pH 6.8, 30% 2-mercaptoethanol, 1% bromophenol blue) was added and samples were boiled at 95°C for 10 minutes. Cellular protein lysates were resolved on Criterion or 4% – 20% Bio-Rad precast SDS-PAGE gels and transferred to PVDF membranes (Bio-Rad). Membranes were saturated and proteins were blotted with antibodies: Rabbit anti-STING (D2P2F) and Rabbit-IgG HRP-linked in 5% non-fat dry milk, PBS 0.1% Tween buffer. ECL signal generated via Clarity Western ECL substrate (Bio-Rad) was recorded on the ChemiDoc-XRS or ChemiDoc Touch Bio-Rad Imager. Data were analyzed and quantified with the Image Lab software (Bio-Rad).

Cell differentiation from bone marrow

Femurs, shin and fibula of female mice were collected immediately after sacrifice, the fat and muscle tissues were removed, the end of the bones were cut with a pair of scissors, and put in a 0.5 mL tubes in which holes were made at the bottom with a needle. The 0.5 mL tube was put in a 1.5 mL tube containing 200 µL of

complete IMDM (Iscove's modified Dulbecco's medium, 10% FBS, penicillin-streptomycin a 1mM 2-mercaptoethanol), and centrifugated at 11,000 *x g* for 10 seconds.
For BMDM cells were seeded at the concentration of 1 million cells per mL in 20 mL total, in a 20 cm non-tissue culture treated plates in BMDM culture media (RPMI GlutMAX, 10% FBS, penicillin-streptomycin, 1 mM 2-mercaptoethanol, 1 mM sodium pyruvate, non-essential amino acids, HEPES, 10 ng/mL human M-CSF (Miltenyi Biotec). Adherent cells were detached with 5 mM EDTA in PBS at day 6. Differentiation was analyzed by staining with anti-CD11b and anti-F4/80 followed by cytometry analysis.
For BMDC (GMCSF), cells were plated in 20 cm non-tissue culture treated plates, at a concentration of 1 million cells per mL in 20 mL, in IMDM containing conditioned supernatant from J558 cells as described *(43)*. At day 4, non-adherent cells were collected, and loosely adherent cells were collected with 5 mM EDTA in PBS. Non-adherent and loosely adherent cells were combined and seeded at the concentration of 0.5 million cells per mL in 20 mL. At day 7, non-adherent cells were discarded, loosely adherent cells were collected with PBS-EDTA and replated at concentration of 0.5 million cells per mL in 20 mL. At day 10 non-adherent cells were discarded, loosely adherent cells were collected with PBS-EDTA. Differentiation was analyzed by staining with anti-CD11b and anti-CD11c followed by cytometry analysis.
For BMDC (FLT3L), bone marrow was isolated as described above, and plated in 6-well cell culture plates at the concentration of 1.5 million cells per mL in 4 mL total of complete IMDM medium supplemented with FLT3L (200 ng/ml). At day 10 of differentiation, the loosely adherent cells were harvested using PBS/EDTA and differentiation was checked by staining for MHC-II, CD11c, B220, and CD24 markers.

***In vivo* antibody depletion**
For $CD8^+$ and NK1.1 depletions studies, B16-OVA tumor bearing mice were treated with 200 µg of anti-CD8α monoclonal antibody or 200 µg of anti-NK1.1 monoclonal antibody or 200 µg of isotype control antibody two times prior and four times after i.t. treatment with STING agonists. To confirm the cell depletion, PBMC were stained according to standard protocols before depletion, at day 7 and day 17. Briefly, cells were surface-stained in 100 µL antibody-mix in FACS buffer: CD19 (clone 6D5), TCR-b (clone H57-597), CD4 (clone RM4-5), CD8 (clone 53-6.7) and NK1.1 (clone PK136). For Treg (Foxp3+CD25+ cells) depletion, MCA-OVA tumor bearing mice were treated with 200 µg of anti-mCTLA4-mIgG2a monoclonal antibody or 200 µg of isotype control antibody three times at days 6, 9 and 12 after tumor engraftment. To confirm the Treg depletion, spleen and tumor cells were stained according to standard protocols 48 hours after the last antibody injection. Briefly, cells were surface-stained in 100 µL antibody-mix in FACS buffer: CD45.2 (clone 104), CD19 (clone 6D5), TCR-b (clone H57-597), CD4 (clone RM4-5), CD8 (clone 53-6.7) and CD25 (clone PC61), followed by an intracellular staining in 50 µL with anti-Foxp3 (clone FJK-16s) and anti-Ki67.

ELISPOT Assay
T cell responses were assessed by IFN-γ ELISPOT 10 days after the first i.t. injection of cGAMP-VLP, synthetic CDNs or PBS. Mice were bled from the retro-orbital sinus. PBMCs were isolated from whole blood by lysing the red blood cells with an ammonium chloride lysis buffer (NH_4Cl 1.5 M, $NaHCO_3$ 100 mM, EDTA 10 mM). $2x10^5$ PBMCs were plated per well in the RPMI medium containing 10% FBS and 1% penicillin-streptomycin. PBMCs were stimulated overnight with media as a negative control, Dynabeads mouse T-activator CD3/CD28 (GIBCO) as a positive control, 10 µg/mL OVA-I 257-264 peptide (SIINFEKL) or 40 µg/mL OVA-II 265-280 peptide (TEWTSSNVMEERKIKV) or 10 µg/mL p15E peptide (KSPWFTTL) or 10 µg/mL DBy 608-622 peptide (NAGFNSNRANSSRSS) or 10 µg/mL UTy 246-254 (WMHHNMDLI). Spots were developed using mouse IFN-γ ELISPOT antibody pair (Diaclone) according to the manufacturer's instructions. The number of spots was enumerated using an ImmunoSpot analyzer and evaluated by subtracting the specific values from the negative control spot number of each sample.

Stimulation of cells with CDNs and cGAMP-VLP
100,000 of the indicated cells were seeded in flat bottom 96-well plates in 200 µL and incubated for few hours until attached to the plate. 100 µL were removed and replaced with serial dilutions of ADU-S100, 2'3'-

cGAMP, cGAMP-VLP or empty VLP. Cells were incubated for 18 hours (37°C, 5% CO_2), and the production of IFN-α and IFN-β were measured in the supernatant.

LEGENDplex Assay

Serum samples were collected three hours after the first STING agonist injection and analyzed for inflammatory cytokines (IFN-α, IFN-ß, TNF-α and IL-6) using a LEGENDplex Mouse Inflammation Panel (BioLegend). For cell culture supernatants, IFN-α and IFN-β concentration were measured using a LEGENDplex Mouse Type 1/2 Interferon Panel (reference 740636). Data was acquired on a FACS Verse (BD Biosciences) and analyzed with BioLegend's LEGENDplex Data Analysis Software. The standard curve regression was used to calculate the concentration of each target cytokine.

Immune cell composition and activation analysis by flow cytometry

All mice from the STING agonist-treated groups (cGAMP-VLP and ADU-S100) and vehicle-treated group were sacrificed 24 hours after the last intratumoral injection. Spleen, draining/non-draining lymph nodes and tumors were excised. Splenocytes were isolated by pressing the spleen through a 40-µm cell strainer, axillary or inguinal LNs were dissected, pierced once with fine tip forceps, and collected into RPMI on ice. For the splenocytes, RPMI was replaced with 2 mL enzymatic solution of CO2-independent medium containing 1 mg/mL liberase (Sigma) and 20 µg/mL DnaseI (Roche), and incubated for 30 minutes in a 37°C incubator with gentle agitation. After 30 minutes, red blood cells were lysed using an ammonium chloride lysis buffer as described above. Cells were pelleted (300 *x g*, 10 minutes, 4°C) and resuspended in ice cold FACS buffer containing 0.5% BSA in PBS. Excised tumors were collected in RPMI supplemented with 10 % FBS and cut into small pieces. Tumor pieces were digested with 1 mg/mL liberase (Sigma) and 20 µg/mL DnaseI (Roche) with gentle continuous agitation (using mouse tumor dissociator gentleMACS). After 40 minutes digestion at 37°C, cells were passed through a 70-µm filter, washed by RPMI supplemented with 10 % FBS, and resuspended in FACS buffer. Single cells were stained according to standard protocols. Briefly, for the immune cell composition analysis, cells were surface-stained in 50 µL antibody-mix in FACS buffer: CD45.2 (clone 104), CD19 (clone 6D5), TCR-β (clone H57-597), CD4 (clone RM4-5), CD8 (clone 53-6.7), CD62L (clone MEL-14), CD69 (clone H1.2F3), CD44 (clone IM7), CD25 (clone PC61), NK1.1 (clone PK136), Nkp46 (clone 29A1.4), CD172a (clone P84), CD11b (clone M1/70), CD11c (Invitrogen), MHC-2 (clone M5/114.15.2), F4/80 (clone BM8), XCR1 (clone ZET), CD64 (clone X54-5/7.1), CD26 (clone H194-112) and CD86 (clone GL1). For the analysis of dendritic cell composition and activation, cells were stained with antibodies against: CD45.2 AF700, TCR-β PE-Cy7, CD19 PE-Cy7, NKp46 PE-Cy7, MHC-II eFluor450, CD11b APC-Fire750, CD11c PECF594, XCR1 BV650, CD172a eF710, CD64 APC, CD86 BUV395, Isotype IgG2a k BUV395, CD80 PE, Isotype IgG2 k PE. For intracellular staining, cells were fixed for 30 minutes on ice using IC Fixation Buffer from Foxp3/Transcription Factor Staining Buffer Set, washed with 1X permeabilization buffer, stained and resuspended in FACS buffer containing anti-Foxp3 (clone FJK-16s) and anti-Ki67. Dead cells were excluded using fixable viability stain according to the manufacturer's instructions. Single-cell suspensions were then analyzed by flow cytometry using FACS LSRFortessa analyzer (BD Biosciences). For the analysis of the relative amounts of OST-STING in dendritic cells and macrophages, splenocytes were stained with antibodies directed against CD11b (clone M1/70) and CD64 (clone X54-5/7.1), permeabilized with BD Cytofix/Cytoperm (BD Biosciences) for 30 min at 4°C, stained with 1/400 or 1/800 dilutions of Strep-Tactin APC (IBA GmbH) and analyzed by flow cytometry.

Analysis of human samples

Head and neck squamous cell carcinoma tumor and lymph node samples were harvested from operative specimens of two patients treated by primary surgery at the Institut Curie. Both patients were smoker-drinkers and had HPV-negative cancers: one 53 years old female had a pT2N2a oropharyngeal tumor and one 58 years old male had a cT4aN0 oral cavity tumor. The samples were obtained with patients consent in accordance with the principles of good clinical practice and the declaration of Helsinki, after study approval from the internal

review Board of the Institut Curie. The male patient was included in the biobanking clinical trial SCANDARE (NCT03017573).

Tumor (T) and lymph node (N) samples were cut into 15 to 20 mg fragments. Samples were cultured at 37°C in 48-wells plates (Costar 3548) in 250 µL of culture media made of RPMI 1640 Glutamax (Life Technologies, 61870-010) with 10% FBS (Hyclone, CH30160.03), 1% Sodium Pyruvate (Gibco, 11360-039), 1% MEM non-essential amino acids (Gibco, 11140-050), and 100 U/mL Penicillin/Streptomycin (Gibco, 15140-122). Stimulation was performed using 200 ng/mL of cGAMP-VLP and 50 µg/mL of 2'3'-c-di-AM(PS)2(Rp,Rp) (Invivogen, tlrl-nacda2r-s) respectively. Depending on sample size, fragments were placed in two to four wells per condition. After 24 hours, tissue samples were collected for flow cytometry analysis and supernatant was collected for multiplexed cytokine analysis.

T and N samples from the same condition were pooled, mechanically and enzymatically digested in CO2-independent medium (Gibco) containing 5% FBS (HyClone), with three enzymes: 2 mg/mL collagenase I (C0130, Sigma), 2 mg/mL hyaluronidase (H3506, Sigma) and 25 µg/mL DNAse (Roche). After three rounds of 15 minutes incubation in a 37°C shaker separated by pipetting, samples were filtered on 40-µm cell strainer (Fischer Scientific) and washed twice with PBS 1X (Gibco) with 2 mMEDTA (Gibco) and 1% decomplemented human serum (BioWest). Single-cell suspensions were stained at 4°C for 15 minutes with antibodies: CD14 FITC, PDL1 PerCP eFluor710, Isotype IgG1 k PerCP eFluor710, CD141 APC, CD3 Alexa700, CD19 Alexa700, CD56 Alexa700, CD45 APC-Cy7, CD83 BV605, Isotype IgG1 k BV605, CCR7 PE, Isotype IgG2a k PE, CD11c PECF594, CD1c/BDCA1 PC7, HLA-DR BUV395. After two washes, cells were stained with DAPI (Miltenyi Biotec) and immediately phenotyped on a LSRFortessa (BD Biosciences). Data was analyzed with FlowJo V10.

The supernatant from the T and N samples from the same condition were pooled, filtered (0,22 µm filter, SLGP033RB, Millipore), diluted 1:2 in the same RPMI-enriched media as used for the 24 hours incubation, and stored at -80°C. IFN-α, IFN-β, and TNF-α measures were obtained using the human premixed multi-analyte kit (R&D systems). Data were acquired with a Bio-Plex 200 plate reader and analyzed with the Bio-Plex Manager 6.1 software (Bio-Rad Laboratories).

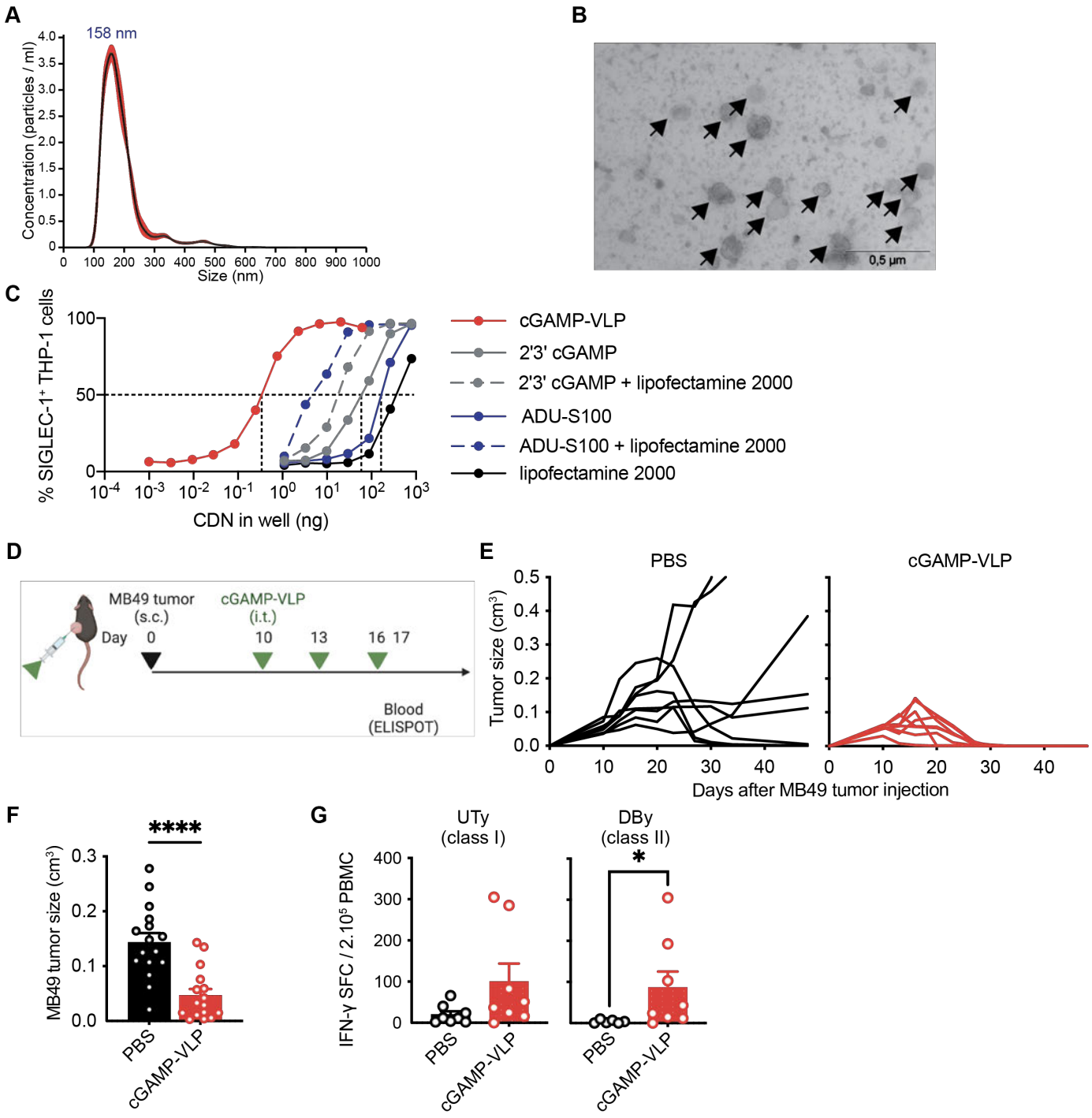

Fig. S1. cGAMP-VLP induces antigen-specific anti-tumor immune responses by intra-tumoral injection.
(A) Size distribution of purified cGAMP-VLP analyzed by Nanoparticle Tracking Analysis. Line at mean, red shading at 1 standard error of the mean (representative data of $N = 21$ experiments). **(B)** Electron microscopy image of purified cGAMP-VLP. Scale bars at 0.5 µm. Arrows point to cGAMP-VLP. **(C)** SIGLEC-1 induction in THP-1 by increasing concentrations of cyclic dinucleotide (CDN) in the form of cGAMP-VLP, soluble 2'3'-cGAMP or soluble ADU-S100, with or without lipofectamine. Lipofectamine 2000 alone condition is plotted at the doses equivalent to the conditions with CDN. Dotted lines indicate CDN dose at 50% SIGLEC-1+ cells. **(D)** Overview of the experimental design. Treatments were started on tumors of 50 mm^3 average volume per group at day 10. Mice were treated at days 10, 13 and 16 with cGAMP-VLP or PBS injected by the i.t. route. **(E)** Growth curves of individual MB49 tumors ($N = 8$ mice per group). **(F)** Size of tumor 17 days after tumor implantation in treated mice (line at mean + SEM, $N = 12$ mice per group combined from 2 independent experiments, Mann-Whitney test). **(G)** T cell responses against UTy (class I peptide) and DBy (class II peptide) in blood of mice 20 days after tumor implantation, assess by IFN-γ ELISPOT (bar at mean + SEM, $N = 6$ to 8 mice per group, Mann-Whitney test with Dunn post-test).

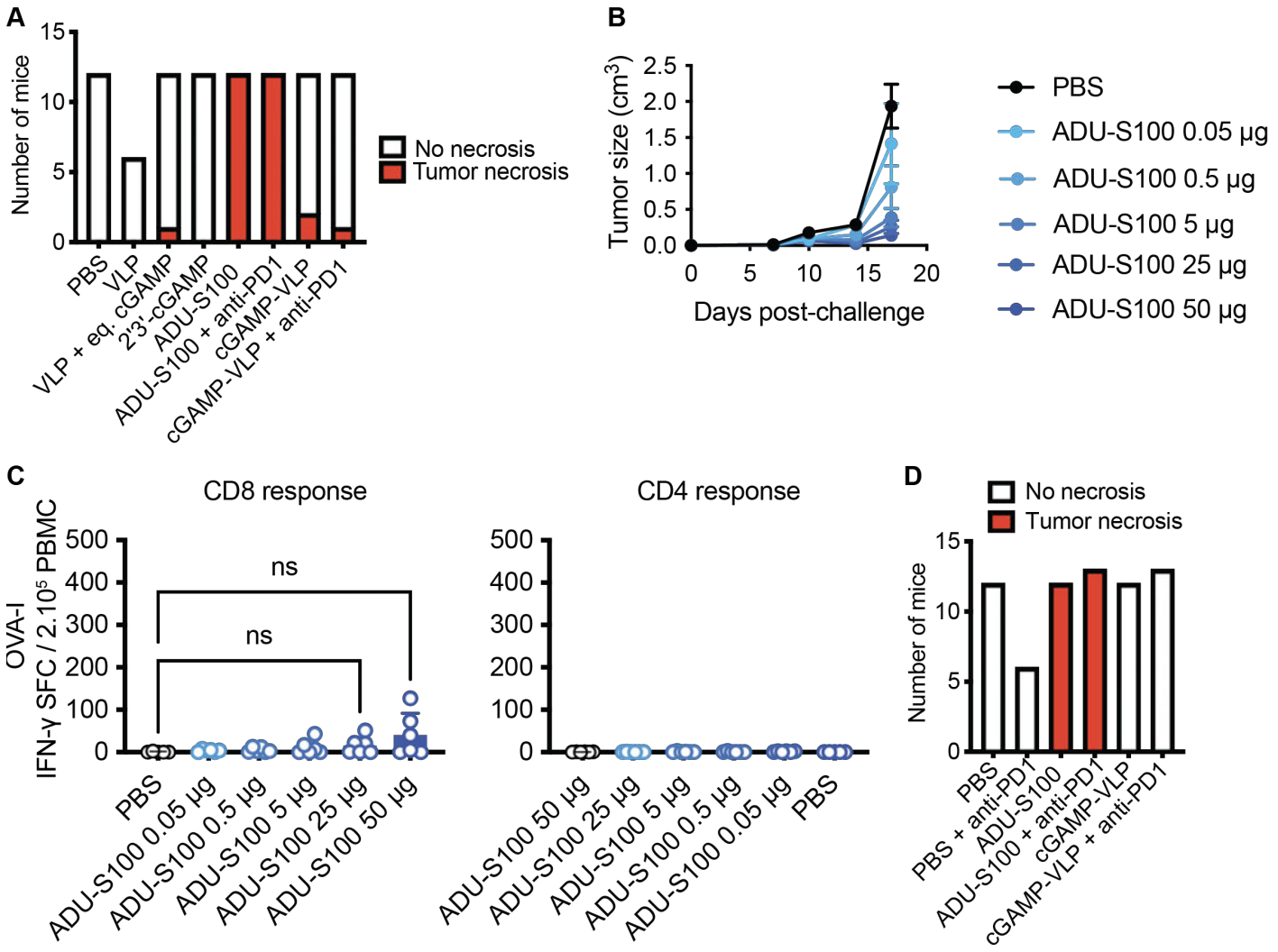

Fig. S2. Responses to lower doses of ADU-S100 and tumor necrosis.
(A) Number of tumor necrosis events after the indicated treatments in single tumor experiments. **(B)** Mean growth over time of B16-OVA tumors treated as indicated by different doses of ADU-S100 (line at mean + SEM, $N = 5$ to 6 mice per group). **(C)** Ova-specific CD8 (OVA-I) and CD4 (OVA-II) T cell responses in blood, assess by IFN-γ ELISPOT (bar at mean + SEM, $N = 5$ to 6 mice per group, Kruskal-Wallis test with Dunn post-test). **(D)** Number of necrosis events in the injected tumor after the indicated treatments in dual tumor experiments.

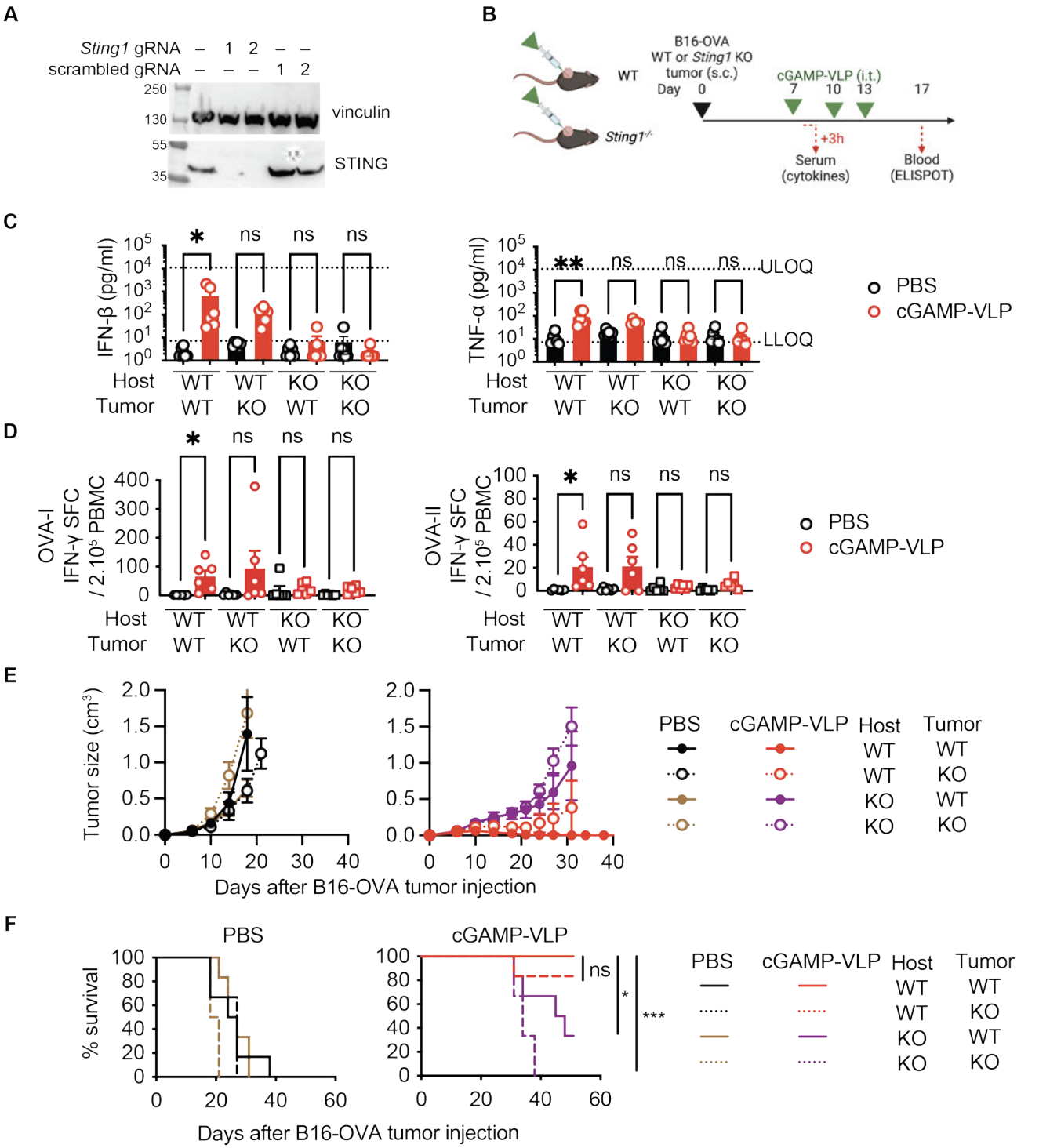

Fig. S3. STING in the host is the main contributor to the anti-tumor effect of cGAMP-VLP.
(A) Western blot of STING and vinculin in B16-OVA WT and *Sting1* KO cells as indicated ($N = 2$, one representative experiment is shown). **(B)** Overview of the experimental design. Treatments were initiated on palpable tumors (15-20 mm^3 range). **(C)** Concentrations of IFN-β and TNF-α in the serum of B16-OVA WT and B16-OVA *Sting1* KO tumor-bearing mice 3 hours after treatment (bar at mean + SEM, $N = 6$ mice per group, Kruskal-Wallis with Dunn post-test, LLOQ = lower limit of quantification, ULOQ = upper limit of quantification). **(D)** Ova-specific CD8 (OVA-I) and CD4 (OVA-II) T cell responses in blood, assessed by IFN-γ ELISPOT (bar at mean + SEM, $N = 6$ mice per group, Kruskal-Wallis test with Dunn post-test). **(E)** Size over time of B16-OVA WT and B16-OVA *Sting1* KO tumors treated as indicated (line at mean ± SEM, $N = 6$ mice per group). **(F)** Survival of B16-OVA tumor-bearing mice treated as indicated (log-rank Mantel-Cox test).

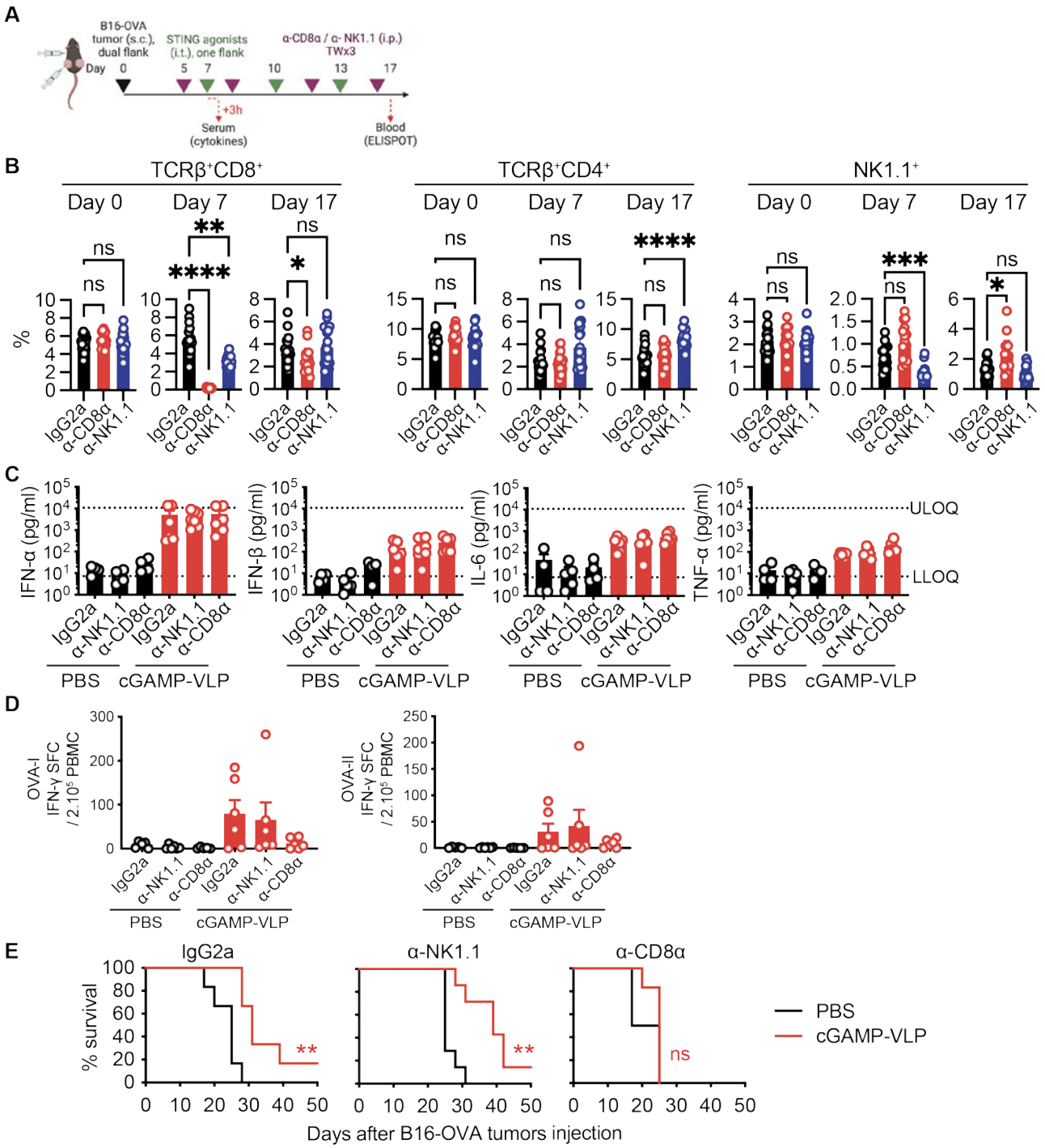

Fig. S4. The anti-tumor effect of cGAMP-VLP requires CD8⁺ T lymphocytes but not NK cells.
(A) Evaluation of the role of CD8⁺ T cells and NK cells, overview of the experiment. Mice were randomized at day 7 and treated by i.t. injection at days 7, 10 and 13 with PBS, 50 µg ADU-S100 or 50 ng cGAMP-VLP. Treatments were initiated on palpable tumors. **(B)** Fraction of CD8⁺ T cells, CD4⁺ T cells and NK cells in the blood at days 0, 7 and 17 after injection with isotype, anti-CD8α or anti-NK1.1 (bar at mean + SEM, *N* = 18 to 21 mice per group, Kruskal-Wallis with Dunn post-test). **(C)** Concentrations of IFN-α, IFN-β, IL-6 and TNF-α in the serum of B16-OVA dual tumor-bearing mice 3 hours after first injection of cGAMP-VLP or PBS, in mice treated with antibodies as indicated (bar at mean + SEM, *N* = 4 to 7 mice per group, LLOQ = lower limit of quantification, ULOQ = upper limit of quantification). **(D)** Ova-specific CD8 (OVA-I) and CD4 (OVA-II) T cell responses in blood of mice treated as indicated, 17 days after tumor implantation, assess by IFN-γ ELISPOT (bar at mean + SEM, *N* = 5 to 6 mice per group). **(E)** Survival of B16-OVA dual tumor-bearing mice treated as indicated (log-rank Mantel-Cox test).

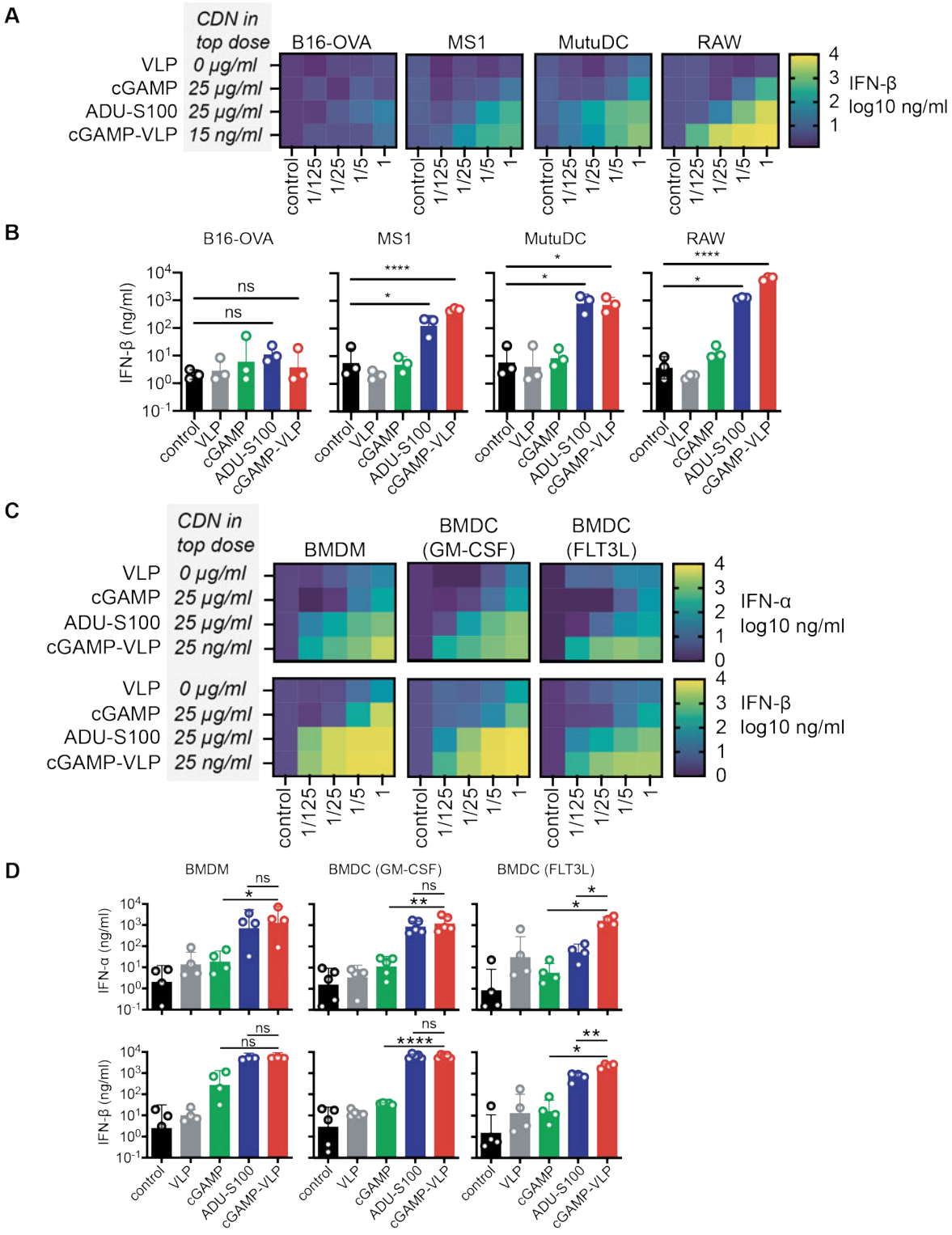

Fig. S5. Response of cell lines and dendritic cells to cGAMP-VLP.
(A) Production of IFN-β by B16-OVA, MS1, MutuDC and RAW cell lines after stimulation with dose titration of VLPs, cGAMP, ADU-S100 and cGAMP-VLP starting at the indicated top dose (averages from $N = 3$ independent experiments). **(B)** Statistical analysis of IFN-β at dilution 1/5 (bar at mean + SEM, $N = 3$ independent experiments, one-way ANOVA with Tukey post-test on log-transformed data). **(C)** Production of IFN-α and IFN-β by BMDM, BMDC (GM-CSF) and BMDC (FLT3L) after stimulation with dose titration of VLP, cGAMP, ADU-S100 and cGAMP-VLP at the indicated top dose (averages from $N = 4$ or 5 independent experiments). **(D)** Statistical analysis of IFN-α and IFN-β at dilution 1/5 (bar at mean + SEM, $N = 4$ or 5 independent experiments, one-way ANOVA with Tukey post-test on log-transformed data).

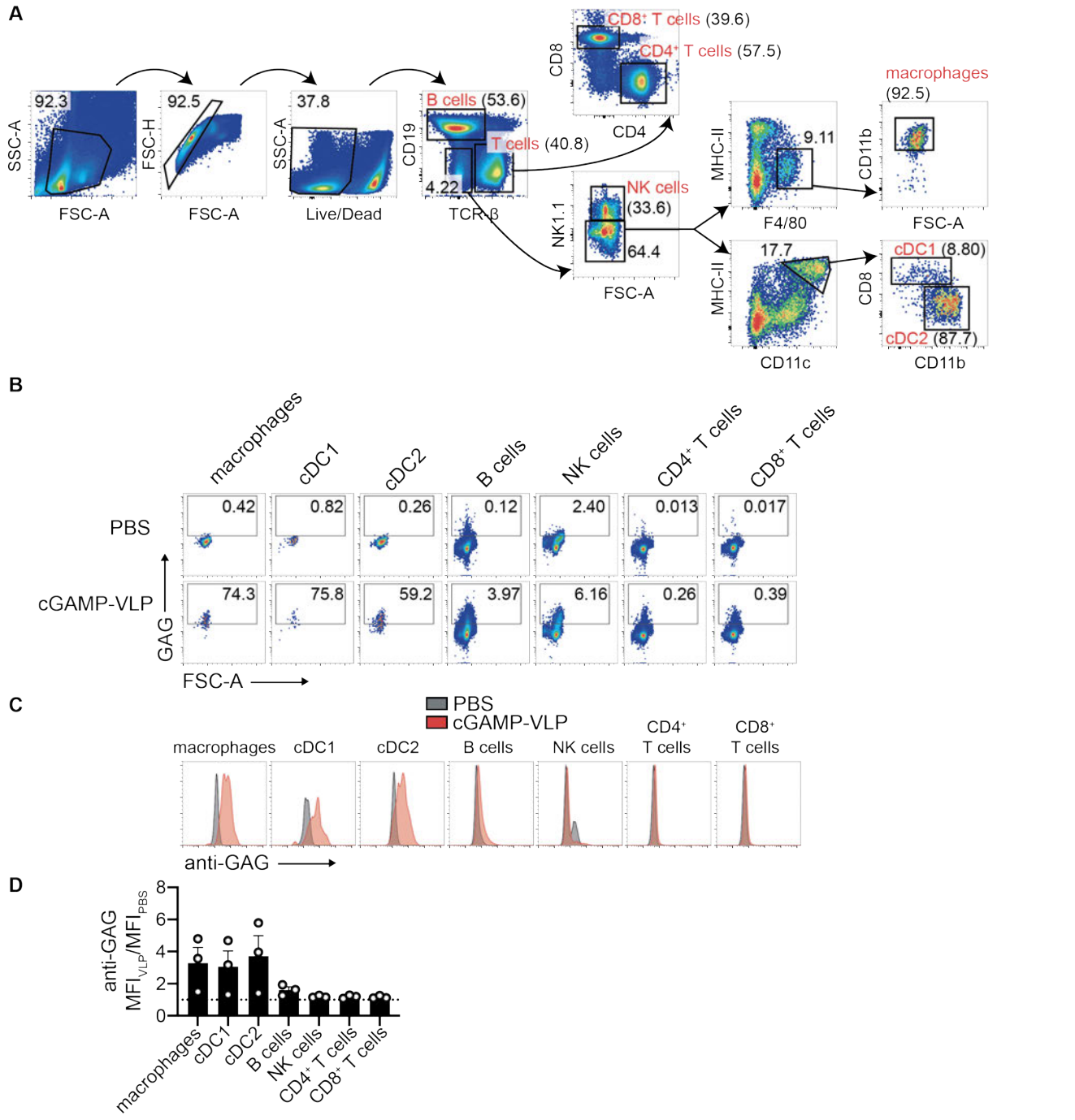

Fig. S6. Capture of cGAMP-VLP by splenocytes.
(A) Gating strategy of immune cells subsets for cGAMP-VLP capture experiments (representative of N = 3 independent experiments). **(B)** Anti-GAG staining and forward scatter in the indicated immune cells from splenocytes treated with PBS or cGAMP-VLP (representative of N = 3 independent experiments). **(C)** Overlaid anti-GAG staining in the indicated immune cells from splenocytes treated with PBS or cGAMP-VLP (representative of N = 3 independent experiments). **(D)** Ratio of anti-GAG mean fluorescence intensity for cGAMP-VLP over PBS (bar at mean + SEM, N = 3 independent experiments).

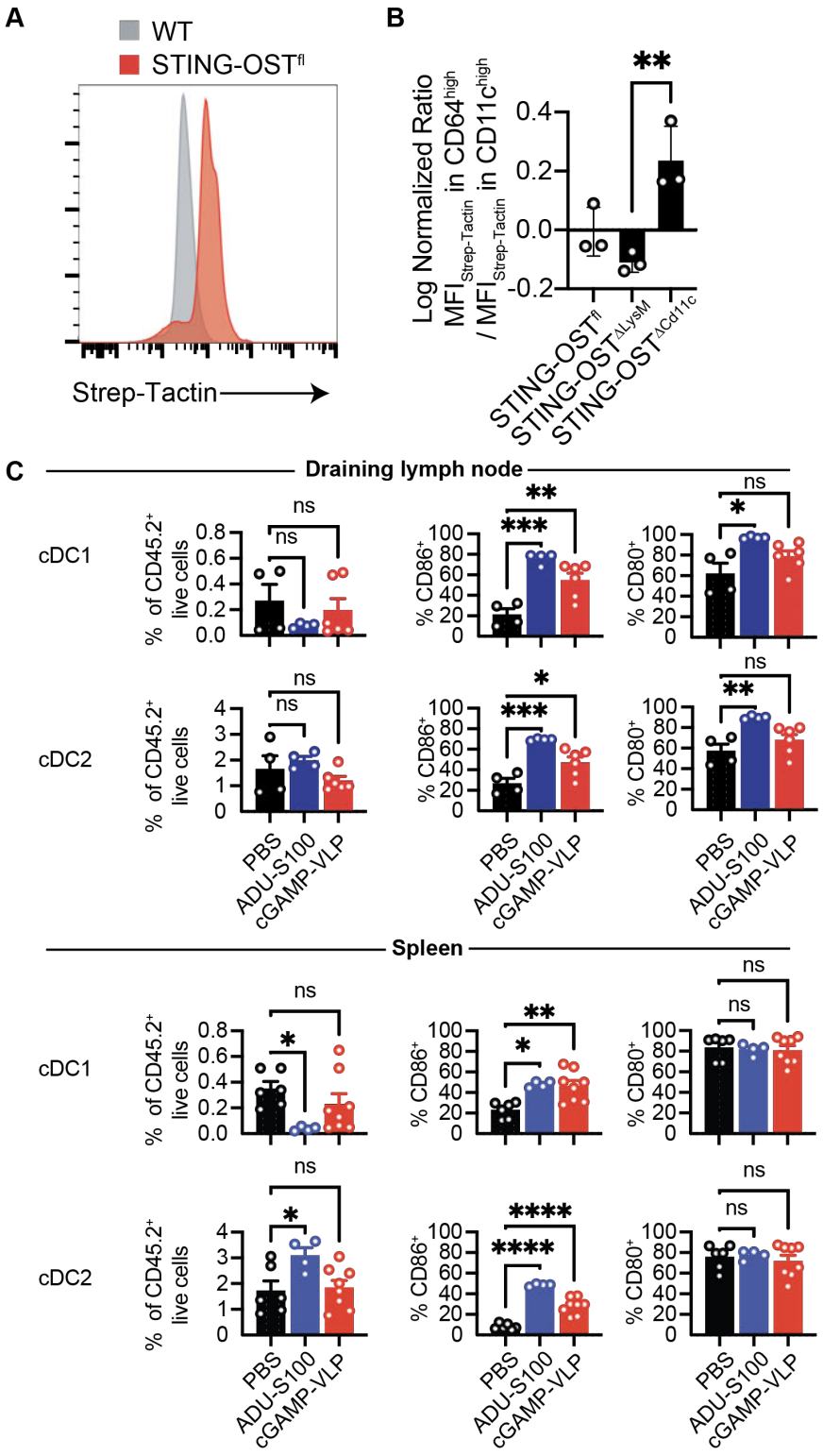

Fig. S7. Preferential deletion of STING in macrophages or dendritic cells and analysis of cDC1 and cDC2 in draining lymph node and spleen.
(A) Representative Strep-Tactin staining in total live single cells in spleen of WT and STING-OST^{fl} mice. **(B)** Relative Strep-Tactin staining in CD64^{high} and CD11c^{high} live single cells in spleen of the indicated mouse strains ($N = 3$ combined from 2 independent experiments, ANOVA with Tukey test). **(C)** Frequency of cDC1 (%MHC-II$^+$CD11c$^+$XCR1$^+$ within CD45.2$^+$ live cells), cDC2 (%MHC-II$^+$CD11c$^+$CD172a$^+$ within CD45.2$^+$ live cells), CD80$^+$ and CD86$^+$ cells on cDC1 and cDC2 (based on isotype) in draining lymph node (upper panel) and spleen (lower panel) of B16-OVA tumor-bearing mice treated as indicated. Data combined from 3 independent experiments ($N = 4$ to 8 mice per group, one-way ANOVA with Tukey test).

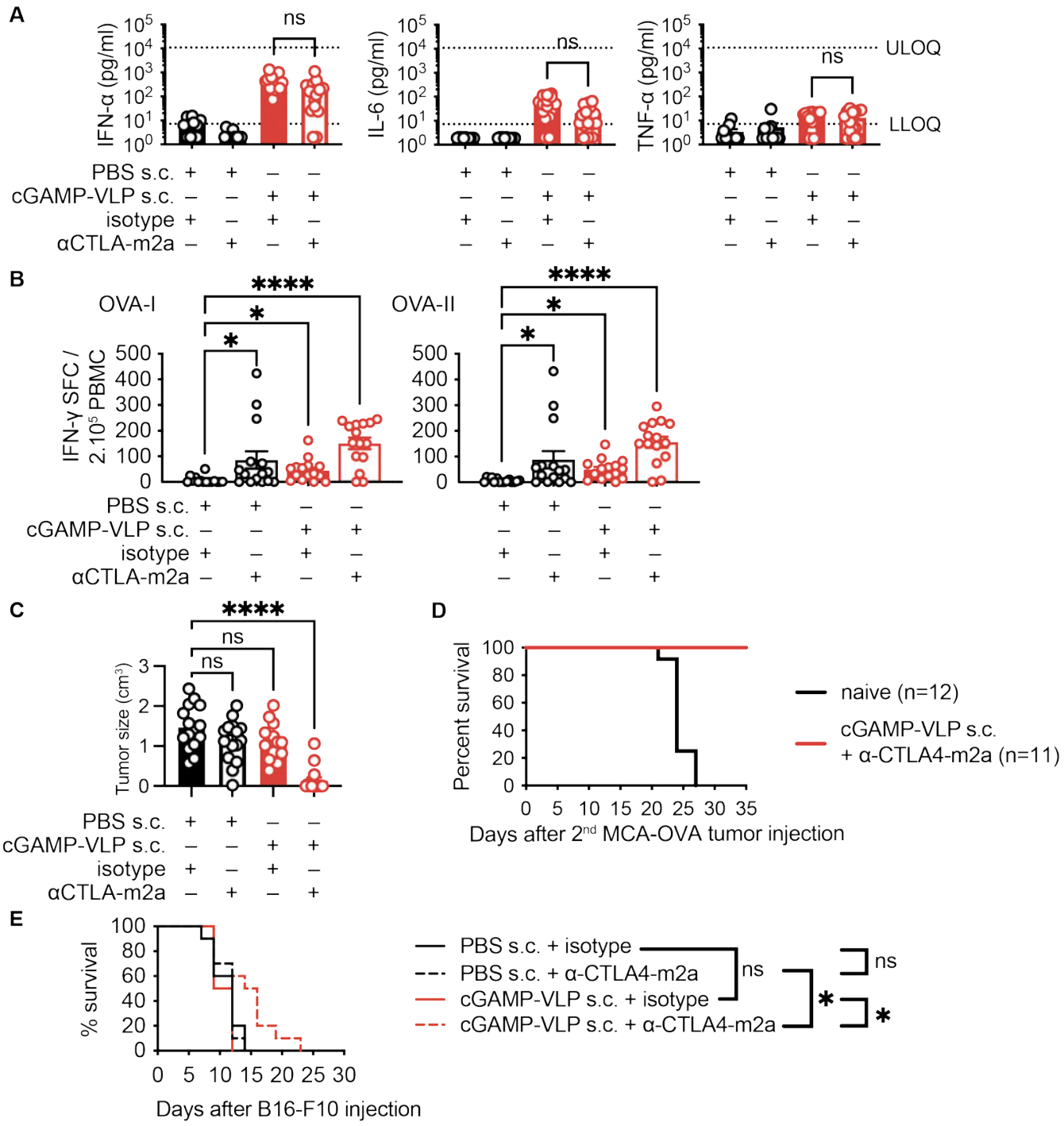

Fig. S8. Additional results for the response to cGAMP-VLP combined with anti-CTLA-m2a.
(A) Concentrations of IFN-α, IL-6 and TNF-α in the serum of MCA-OVA tumor-bearing mice 3 hours after the first treatment with PBS or 50 ng cGAMP-VLP injected by s.c., and i.p. injection of αCTLA4-m2a or isotype. Treatments were started on tumors of 50 mm^3 average volume per group (bar at mean + SEM, N = 11 to 15 mice per group, combined from 2 independent experiments, Kruskal-Wallis with Dunn post-test, LLOQ = lower limit of quantification, ULOQ = upper limit of quantification). **(B)** Ova-specific CD8 (OVA-I) and CD4 (OVA-II) T cell responses in blood of mice 16 days after tumor implantation, assess by IFN-γ ELISPOT (bar at mean + SEM, N = 15 mice per group, combined from 2 independent experiments, Kruskal-Wallis with Dunn post-test). **(C)** Size of tumor 28 days after tumor implantation in treated mice (line at mean + SEM, N = 15 mice per group combined from 2 independent experiments, Mann-Whitney test). **(D)** Survival of mice after secondary challenge. In complete responding mice, MCA-OVA cells were injected 55 days from the first injection of tumor cells and treatments (combined from 2 experiments, log-rank Mantel-Cox test). **(E)** Survival of B16-F10 tumor-bearing mice treated as indicated (N = 10 mice per group, from one experiment, log-rank Mantel-Cox test).

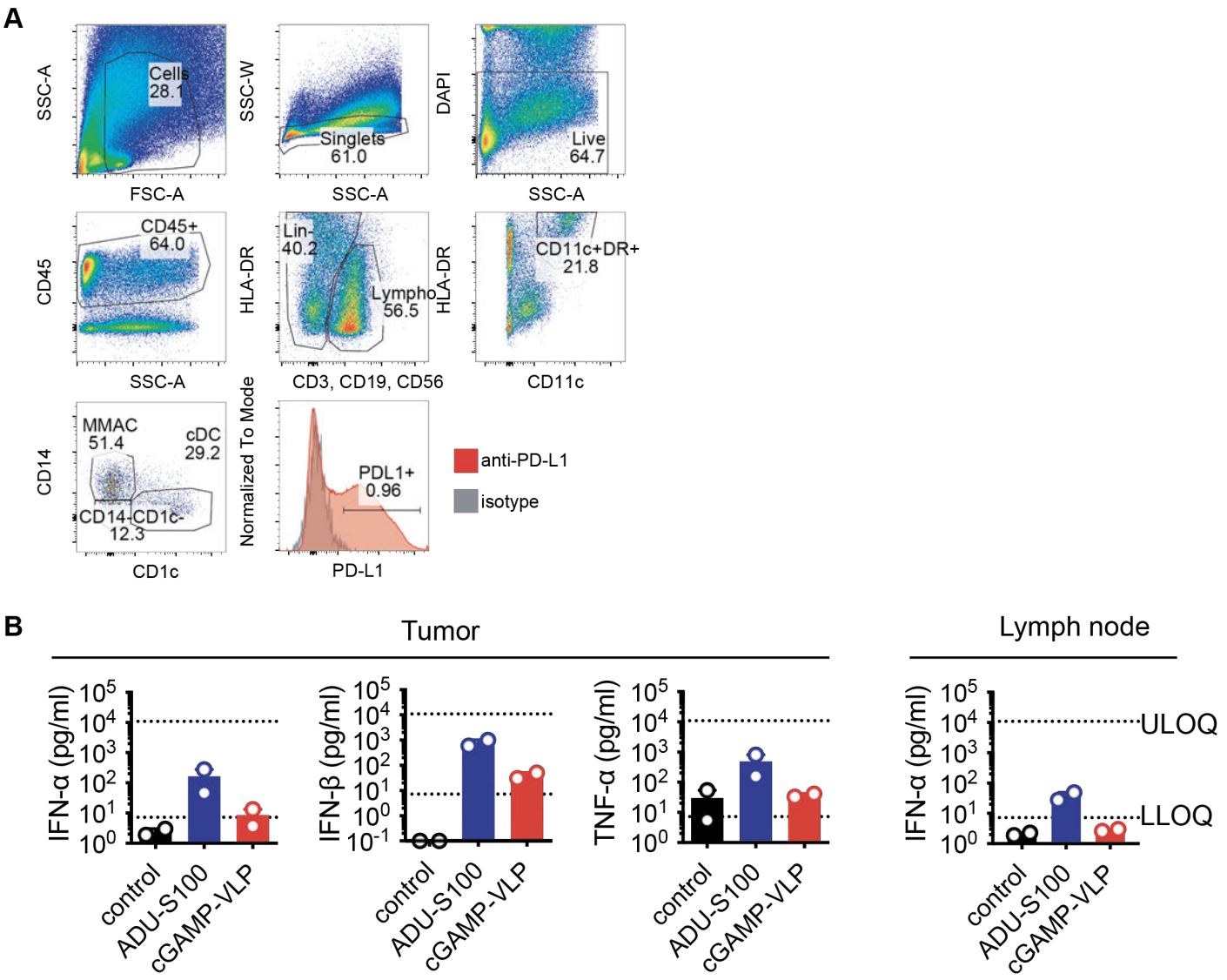

Fig. S9. Additional results for the stimulation of STING in human cancer patient samples.
(A) Gating strategy of immune cells stimulated with cGAMP-VLP (lymph node sample, representative of $N = 2$ independent experiments from 2 different patients). **(B)** Concentrations of IFN-α, IFN-β and TNF-α in the supernatants (bar at mean, $N = 2$ samples, combined from 2 independent experiments, LLOQ = lower limit of quantification, ULOQ = upper limit of quantification).

Table S1. List of cell lines used in the study.

Cell line	Source	References
B16-OVA	K.L. Rock lab, Dana Farber Cancer Institute	Falo LD Jr, et al. (1995)
B16-OVA WT	This study	N/A
B16-OVA *Sting1* KO	This study	N/A
MCA-OVA	Clotilde Thery lab, Institut Curie	Zeelenberg, I.S., et al. (2008)
MB49	Clotilde Thery lab, Institut Curie	Mohamed El Behi, et al. (2013)
B16-F10	Crown Bioscience	N/A
293T	ATCC	CRL-3216
RAW	Dan Littman lab, NYU	N/A
MS1	Michel Gilliet lab, CHUV, Lausanne	N/A
THP-1	ATCC	TIB-202
MutuDC	Sebastian Amigorena lab, Institut Curie	N/A

Table S2. List of plasmids, peptides and proteins used in the study.

Plasmids, peptide or protein	Source	References
OVA-I 257-264	GeneCust	N/A
OVA-II 265-280	GeneCust	N/A
DBy 608-622	GeneCust	N/A
UTy 246-254	GeneCust	N/A
2'3' cGAMP	Invivogen	Cat#tlrl-cga23
ADU-S100	Invivogen	Cat#tlrl-nacda2r
Protease inhibitor	Roche	1187358001
FLT3L	Peprotech	250-31L
PEIpro	Ozyme	POL115-010
pVAX1	ThermoFisher	V26020
pVAX1-VSVG-INDIANA2	This study	N/A
pVAX1-cGAS	This study	N/A
psPAX2	AddGene	12260
pCMV-VSV-G	AddGene	8454
lentiCRISPR v2	AddGene	52961
pLentiCRISPRv2-mSTING-gRNA_1	This study	N/A
pLentiCRISPRv2-mSTING-gRNA_2	This study	N/A
pLentiCRISPRv2-mSTING-scrambled_gRNA_1	This study	N/A
pLentiCRISPRv2-mSTING-scrambled_gRNA_2	This study	N/A

Table S3. List of antibodies used in the study.

Antigen or Antibody	Source	Reference
PD1 (clone RMP1)	BioXcell	Cat#BE0146
Rat IgG2a isotype (2A3)	BioXcell	Cat# BE0089
Anti-CD8α (clone 53-6.7)	BioXcell	Cat#BE0004-1
Anti-NK1.1 (clone PK136)	BioXcell	Cat#BE0036
Rat IgG2a isotype (RG7/1.30)	BioXcell	Cat#BE0251
Anti-mCTLA4-mIgG2a	Invivogen	CTA-42-01
Anti-β-Gal-mIgG2a	Invivogen	10362-42-01
Fixable Viability Dye	eBioscience	Cat#65-0865-14
CD45.2 (clone 104)	BioLegend	Cat#109822
CD19 (clone 6D5)	Invitrogen	Cat#15-0193-82
TCR-β (clone H57-597)	BioLegend	Cat#109222
CD8 (clone 53-6.7)	BD Biosciences	Cat#561093
CD4 (clone RM4-5)	BioLegend	Cat#100552
NK1.1 (clone PK136)	BD Biosciences	Cat#561111
Nkp46 (clone 29A1.4)	eBioscience	25-3351-8
MHC-II (clone M5/114.15.2)	eBioscience	Cat#48-5321-82
F4/80 (clone BM8)	eBioscience	Cat#56-4801-82
CD11b (clone M1/70)	Invitrogen	Cat#12-0112-82
CD11c (PETR)	Invitrogen	Cat#MCD11c17
CD62L (clone MEL-14)	BD Biosciences	Cat#560516
CD44 (clone IM7)	BioLegend	Cat#103028
CD25 (clone PC61)	BioLegend	Cat#102012
CD69 (clone H1.2F3)	BioLegend	Cat#104512
CD64 (clone X54-5/7.1)	BioLegend	Cat#139306
CD26 (clone H194-112)	BioLegend	Cat#137804
CD172a (clone P84)	eBioscience	46-1721-80
XCR1 (clone ZET)	BioLegend	Cat#148220
CD80 (clone 16-10A1)	BD Biosciences	Cat#553769
Isotype IgG2 k (PE)	BD Biosciences	Cat#559277
CD86 (clone GL1)	BD Biosciences	Cat#564199
Isotype IgG2a k (BUV395)	BD Biosciences	Cat#563809
Foxp3 (clone FJK-16s)	BD Biosciences	Cat#48-5773-82
Ki67 (PE)	BD Biosciences	Cat#556027
HIV-1 GAG (KC57)	Beckman Coulter	Cat#6604665
Anti-human SIGLEC-1	Miltenyi	130-098-645
CD14 (FITC)	BD Biosciences	Cat#555397
PDL1 (clone MIH1)	eBioscience	46-5983-42
Isotype IgG1 k (PerCPeFluor710)	eBioscience	46-4717-82
CD141 (clone AD5-14H12)	Miltenyi	130-090-907
CD3 (AF700)	BD Biosciences	Cat#557973
CD19 (AF700)	BD Biosciences	Cat#557921
CD45 (APC-Cy7)	BD Biosciences	Cat#557833
CD56 (AF700)	BD Biosciences	Cat#557919
CD83 (clone HB15e)	BD Biosciences	Cat#740420
Isotype IgG2a k (PE)	BioLegend	Cat#400213
CD11c (clone B-ly6)	BD Biosciences	Cat#562393
CD1c/BDCA1 (clone L161)	BioLegend	Cat#331516
HLA-DR (clone G46-6)	BD Biosciences	Cat#564040
Rabbit anti-STING (D2P2F)	Ozyme	Cat#13647
Rabbit-IgG HRP-linked	Ozyme	Cat#7074S

Table S4. List of commercial assays used in the study.

Commercial kit	Source	References
2'3'-cGAMP ELISA Kit	Cayman Chemical	501700
LEGENDplex Multi-Analyte Flow	BioLegend	Cat#B262462
Murine IFN-γ ELISpot Pair	Diaclone	Cat#870.050.010
Human premixed multi-analyte kit	R&D systems	LXSAHM-06 batch L144686